Acta Geodyn. Geomater., Vol. 21, No. 3 (215), 207–240, 2024
DOI: 10.13168/AGG.2024.0019
journal homepage: https://www.irsm.cas.cz/acta

ORIGINAL PAPER

GIS-BASED LANDSLIDE SUSCEPTIBILITY ASSESSMENT USING RANDOM FOREST AND SUPPORT VECTOR MACHINE MODELS: A CASE STUDY OF CHIN STATE, MYANMAR

Soe Hlaing TUN, Changnv ZENG * and Farhad JAMIL

School of Civil Engineering and Architecture, Henan University of Technology, Zhengzhou 450001, Henan, China

**Corresponding author's e-mail:* zengcnv@126.com

ARTICLE INFO

Article history:
Received 2 July 2024
Accepted 11 September 2024
Available online 24 September 2024

Keywords:
Geographic information system (GIS)
Landslide susceptibility map
Random forest,
Support vector machine
Model performance evaluation and validation
Chin state in Myanmar

ABSTRACT

Chin State in Myanmar experiences frequent landslides annually. This research aimed to construct GIS-based landslide susceptibility maps (LSMs) with two kinds of machine learning models, namely random forest (RF) and support vector machine (SVM). Firstly, a landslide inventory map was constructed by containing 213 landslide locations and randomly chosen 213 non-landslide locations; these location points were randomly divided into the training set (70 %) for the landslide susceptibility prediction model and the testing set (30 %) for the model validation. Secondly, twenty-one landslide conditioning factors were selected, and frequency ratio analysis was used to evaluate the relationship between each class of factors and landslide occurrences. Then, landslide susceptibility prediction modeling by RF and SVM models. Finally, the performance of the two models was evaluated with performance metrics (precision, recall, F1-Score, and accuracy), receiver operating characteristic (ROC) curves, and area under the ROC curve (AUC values). The RF model demonstrated superior performance across performance evaluation metrics, with a precision of 0.864, recall of 0.919, F1-Score of 0.891, and an accuracy of 0.894 on the training set, compared to the SVM model's precision of 0.854, recall of 0.807, F1-Score of 0.830, and accuracy of 0.825. The model validation by the testing set further confirmed that the RF model showed a precision of 0.839, recall of 0.897, F1-Score of 0.867, and an accuracy of 0.871, while the SVM model had a precision of 0.839, recall of 0.839, F1-Score of 0.839, and an accuracy of 0.839. Also, the results of AUC values showed that the RF model (training set AUC = 0.94, testing set AUC = 0.92), and SVM model (training set AUC = 0.89, testing set AUC = 0.88), respectively. Hence, these two landslide susceptibility prediction models demonstrated satisfactory results and good accuracy for LSMs in this research area, and the LSM from the RF model is better than the SVM model according to performance metrics and AUC values results. The resulting maps provide useful information on the likelihood of landslide occurrence, facilitating decision-making in land use planning and disaster management.

1. INTRODUCTION

Landslides occur due to several factors, which encompass precipitation, seismic or volcanic events, human practices like mining and construction, and alterations in soil stability as a result of climate change (Gopi et al., 2023; Hart, 2024; Maodin et al., 2023). These factors can lead to the destabilization of slopes, resulting in the movement of large amounts of earth, rock, and other material down a slope (Thakur and Sharma, 2022). Other factors contributing to landslides comprise the depletion or nonexistence of vertical vegetative composition, the erosion of slopes' bases by rivers, considerable precipitation, seismic activity inducing the liquefaction of slopes, the impact of blasting, and earthwork that alters the slope and imposes new loads on it. Landslides encompass the downward slope displacement of debris, rocks, or earth material caused by the force of gravity. Landslides can also be prompted by human activities, earthquakes, and torrential rainfall (Gopi et al., 2023). The causes and mechanisms of landslides are complex, typically precipitated by the surpassing of driving forces over resisting forces, leading to slope destabilization. (Schuster and Wieczorek, 2018).

The investigation, susceptibility assessment, hazard evaluation, and risk cartography of landslides are important for disaster loss reduction and formulating sustainable land utilization plans (Davies, 2015). These are constructed based on the statistical correlation between environmental conditions and previously recorded landslides. A comprehensive comprehension of the causes and characteristics of landslides is indispensable for precise monitoring, prediction, preparedness, and prevention. Landslides are a pervasive geohazard that can lead to substantial destruction and loss of life. It is crucial to comprehend the factors contributing to landslides and establish techniques for delineating the susceptibility of areas to landslides to mitigate their impact (Badola et al., 2023; Chen and Chen, 2021; Kunwar et al., 2023; Woodard et al., 2023; Zhou et al., 2023). Creating landslide susceptibility zone maps is important for decreasing

Cite this article as: Tun SH, Zeng C, Jamil F: GIS-based landslide susceptibility assessment using random forest and support vector machine models: A case study for Chin State, Myanmar. Acta Geodyn. Geomater., 21, No. 3 (215), 207–240, 2024. DOI: 10.13168/AGG.2024.0019

risk and controlling land use in a region. Different approaches and techniques, such as statistical models and machine learning methods, have been utilized for landslide susceptibility mapping (Chen and Chen, 2021).

Machine learning algorithms have been widely employed in research studies to create maps that predict the likelihood of landslides. The effectiveness of various machine learning algorithms, such as random forest (RF), decision tree (DT), and support vector machine (SVM) (Shahabi et al., 2023); RF, SVM, logistic regression (LR), and extreme gradient boosting (XGBoost) (Kwon et al., 2023; Zhang et al., 2022); SVM, LR, and artificial neural network (ANN) (Zhou et al., 2018); RF, DT, and LR (Gao et al., 2022) has been thoroughly evaluated across different study areas. For landslide susceptibility assessment, these models utilize a diverse array of landslide conditioning factors, including elevation, altitude, aspect, slope angle, inclination angle, dip direction, slope height, plan curvature, profile curvature, profile shape, plane morphology, distance to roads, distance to rivers, distance to faults, stream power index (SPI), sediment transport index (STI), topographic wetness index (TWI), normalized difference vegetation index (NDVI), land use, land cover, landslide volume, rainfall, geology, lithology, soil, soil classification, soil types, cross-sectional type, longitudinal type, vegetation works, vegetation coverage, bedding structure, structure type, the width of the structure, length of the structure, slope stabilization works, slope surface protection works, surface water drainage works, step duration orographic intensification factor (SDOIF), external condition, and influence degree of human activities (Chen and Chen, 2021; Gao et al., 2022; Kwon et al., 2023; Wang et al., 2021; Zhang et al., 2022; Zhou et al., 2018). The wide range of machine learning algorithms and conditioning factors applied in landslide susceptibility assessments across different regions highlights their adaptability and effectiveness. As a significant environmental concern, landslides can be effectively managed using these machine learning models, which are robust in capturing complex interactions.

The application of machine learning and deep learning techniques in landslide susceptibility prediction modeling has garnered significant attention due to their ability to manage complex, multivariate datasets and detect hidden patterns within data, which leads to more accurate predictions (Achu et al., 2023; Nhu et al., 2020a). However, the effectiveness of these models is closely tied to the availability and quality of field data used for training. In regions with limited data, the predictive performance of these models may be compromised (Achu et al., 2023; Zhang and Ling, 2018). Deep learning models, such as deep neural networks (DNN), are highly efficient in landslide susceptibility modeling across various geoenvironmental settings; their moderate performance in data-limited conditions is primarily due to the insufficient amount of field data available for model training (Achu et al., 2023). DNN is a sophisticated, nonlinear, multi-layered architecture designed to process and analyze large, complex datasets, such as those related to landslide conditioning factors. These networks are equipped with advanced hyperparameters that help mitigate overfitting, thereby ensuring the generation of accurate and reliable landslide susceptibility prediction (Achu et al., 2024; Hua et al., 2021). However, the effectiveness of DNN, like many deep learning tools, is highly dependent on the availability of extensive datasets for optimal performance, and their effectiveness diminishes significantly in data-limited conditions (Achu et al., 2024, 2023; LeCun et al., 2015; Sarker, 2021). In light of these considerations, the choice between machine learning models like SVM and RF and more advanced deep learning techniques depends heavily on the specific data context. In regions like Chin State, Myanmar, where field data is limited, a thorough evaluation of the available data and the selected model's capability to generalize from small datasets is crucial. Therefore, while deep learning models may offer theoretical advantages, SVM and RF models remain competitive alternaives, particularly in data-constrained environments, making them suitable choice or landslide susceptibility assessment in such regions.

In the western part of Myanmar, Chin State frequently experiences landslides, which pose a significant natural hazard. This region's rugged terrain, heavy rainfall, and geological characteristics contribute to the high incidence of these devastating events. Landslides can cause substantial loss of life, damage toinfrastructure, and economic repercussions, emphasizing the necessity of comprehending the fundamentalfactors contributing to their occurrence. Despite the critical nature of this issue, previous studies on landslide susceptibility in Chin State have predominantly focused on localized areas such as the vicinity of Hakha (Kyaw Htun et al., 2019; May Thu et al., 2022; Yasukuni and Soe, 2017). These studies have not provided a comprehensive, region-wide assessment that encompasses the diverse environmental conditions and broader geographical context of the entire state.

This research addresses this gap by employing a comprehensive approach that combines geospatial analysis with machine learning models to develop landslide susceptibility maps (LSMs) for the entire Chin State. The novelty of this research is in the application of two advanced machine learning algorithms—Random Forest (RF) and Support Vector Machine (SVM)—to generate highly accurate predictions of landslide-prone areas. Unlike previous studies, this research leverages the strengths of machine learning to handle complex, nonlinear relationships between the various landslide conditioning factors, providing a more nuanced understanding of landslide susceptibility across the region. By integrating geospatial data with machine learning algorithms, this study offers a more robust

and precise tool for assessing landslide risks, which can significantly enhance disaster management and land-use planning in Chin State.

The research begins with data collection and preparation, involving selecting and evaluating landslide conditioning factors—the variables that influence the occurrence of landslides. Then, the next step lays the substance for the model implementation phase, where the research develops and validates the performance of the landslide susceptibility prediction model. Finally, the culmination of the research is the generation of LSMs, providing a clear visual representation of the areas at risk. This step-by-step process systematically builds the necessary components to achieve the overarching purpose of assessing and mapping the susceptibility of the study area to landslide events. The resulting maps will provide crucial insights for policymakers, aiding in the development of strategies to mitigate landslide risks and enhance community resilience against such natural disasters.

2. STUDY AREA

The study area, Chin State, is situated in western Myanmar, with latitudes 20°30′00″ N–24°30′00″ N and longitudes 92°30′00″ E–94°30′00″ E. The area is 35992.51 square kilometers (13896.78 sq. miles), and its location is shown in Figure 1. Chin State is part of the Indo-Burma Ranges, which are geologically complex and include schist exposed in the ranges (Tin Tin et al., 2023). The Indo-Burman Ranges, also known as the Western Ranges, stretch from the East Himalayan Syntaxis (EHS) towards the south along the eastern coast of the Bay of Bengal up to the Andaman Sea. This region includes the Naga Hills Tract in the northern part, the Chin Hills in the middle area (i.e., Chin state), and the Rakhine Yoma in the southern part (Kyi Khin et al., 2017). The Chin State, located in the Western Ranges, is a mountainous state with steep slopes, unstable geology, and intense monsoon precipitation. Chin State has encountered various forms of slope failures, with numerous areas being at risk of potential landslide hazards. Every year, landslides occur, resulting in damage to roads, bridges, houses, and villages (Kyaw Htun et al., 2019; May Thu et al., 2022; Yasukuni and Soe, 2017). Myanmar faces various natural disasters such as floods, cyclones, earthquakes, tsunamis, and landslides. These natural calamities in Myanmar result in significant economic losses and social impacts (Alvioli et al., 2018). In July 2015, Cyclone Komen caused severe devastation in parts of Myanmar, particularly affecting Chin State, where housing and infrastructure were damaged and destroyed. The state also witnessed a high level of torrential precipitation, leading to thousands of landslides being triggered in Chin State (Alvioli et al., 2018; Dixon et al., 2022; Kyaw Htun et al., 2019; Yasukuni and Soe, 2017). The Chin State's climate falls within the southwest monsoon region, leading to noticeable seasonal variations in the climate. The monsoon period lasts from mid-May to October, with rainfall surpassing 254 mm in the Chin Hills. From November to January, the cool season experiences minimal rainfall; the daily maximum temperatures rarely go beyond 29.4 °C and the minimum temperatures drop to −4 °C. The hot season, from February to May, is dry and sees temperatures frequently exceeding 40.5 °C in the valleys on the eastern side of the region. In the northern part of Chin State, surrounding the towns of Falam and Hakka, extensive areas of forest have been destroyed in these areas, while in the eastern margin and southern Chin Hills, the forest is generally thinner (Kyaw Htun et al., 2019). The northern region of Chin State comprises sedimentary and metasedimentary rocks of the flysch type, categorized into three distinct units based on lithology, stratigraphic position, and faunal content: the Falam Mudstone-Micrite Formation, the Chunsung Mudstone-Turbidite Formation, and the Kennedy Sandstone Formation (Kyaw Htun et al., 2019; United Nations Team, 1979).

3. MATERIALS AND METHODS

The research methodology flow chart is illustrated in Figure 2. The methodology employed for generating the LSMs involved a systematic approach that encompassed 5 main stages: (1) selecting a research area, gathering field investigations, and spatial data collection; (2) comprehensive data preparation, where preprocessing steps were implemented to ensure consistency, accuracy, and compatibility for the landslide inventory map and landslide conditioning factors; (3) determining landslide conditioning factors using frequency ratio analysis; (4) landslide susceptibility modeling by RF and SVM models; and (5) validation of models and comparison of performance among two models with confusion matrix (TP, TN, FP, and FN), performance metrics (precision, recall, F1-Score, and accuracy), receiver operating characteristic (ROC) curves, and area under the ROC curve (AUC values). Finally, the LSMs provided the representation of the probability of landslide occurrence, enabling the identification of very low, low, moderate, high, and very high susceptibility classes within this research area.

3.1. LANDSLIDE INVENTORY MAP

A landslide inventory map can be created through various methodologies, contingent upon the accessible resources, the size of the area under research, and the scope of the research (Guzzetti et al., 2006). The process of mapping a landslide inventory entails the systematic mapping of currently existing landslides within a specific area through the utilization of diverse techniques, including field surveying, interpretation of aerial photographs or Google Earth imagery, analysis of satellite images, thorough examination of literature for historical records of landslides, review of technical and scientific reports, governmental reports, as well as conducting interviews with experts in the field (Addis, 2023; Sivakami et al., 2020; Wubalem, 2022). In this

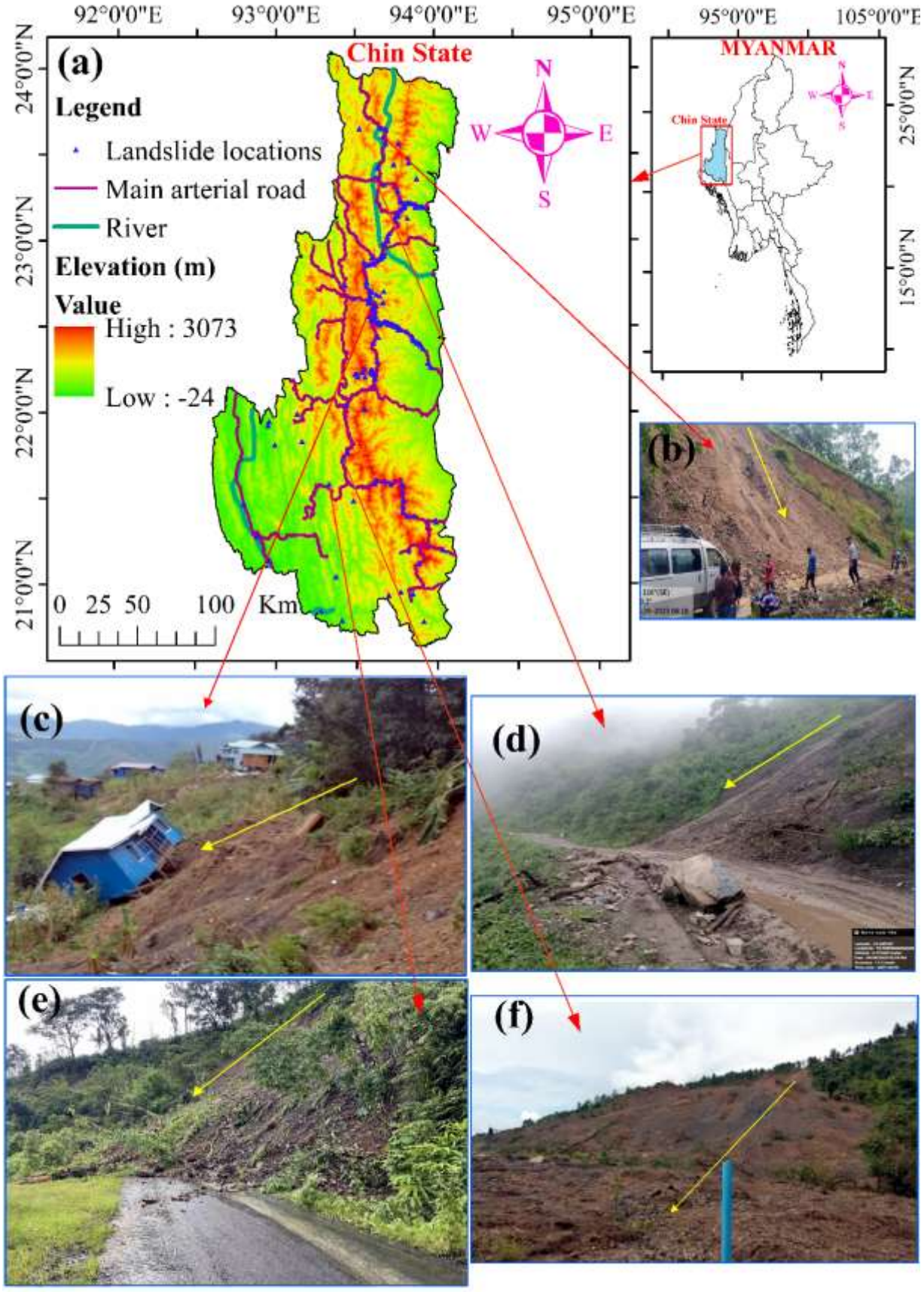

Fig. 1 (a) Study area and landslide inventory map, (b) landslide event on Tedim-Tonzang-Cikha-Khenman road, (c) landslide event in Myohaung ward, Hakha town, (d) landslide event on Tedim-Rihkhawdar road, (e) landslide event on Matupi-Paletwa road, and (f) landslide event on Hakha-Matupi Road, respectively.

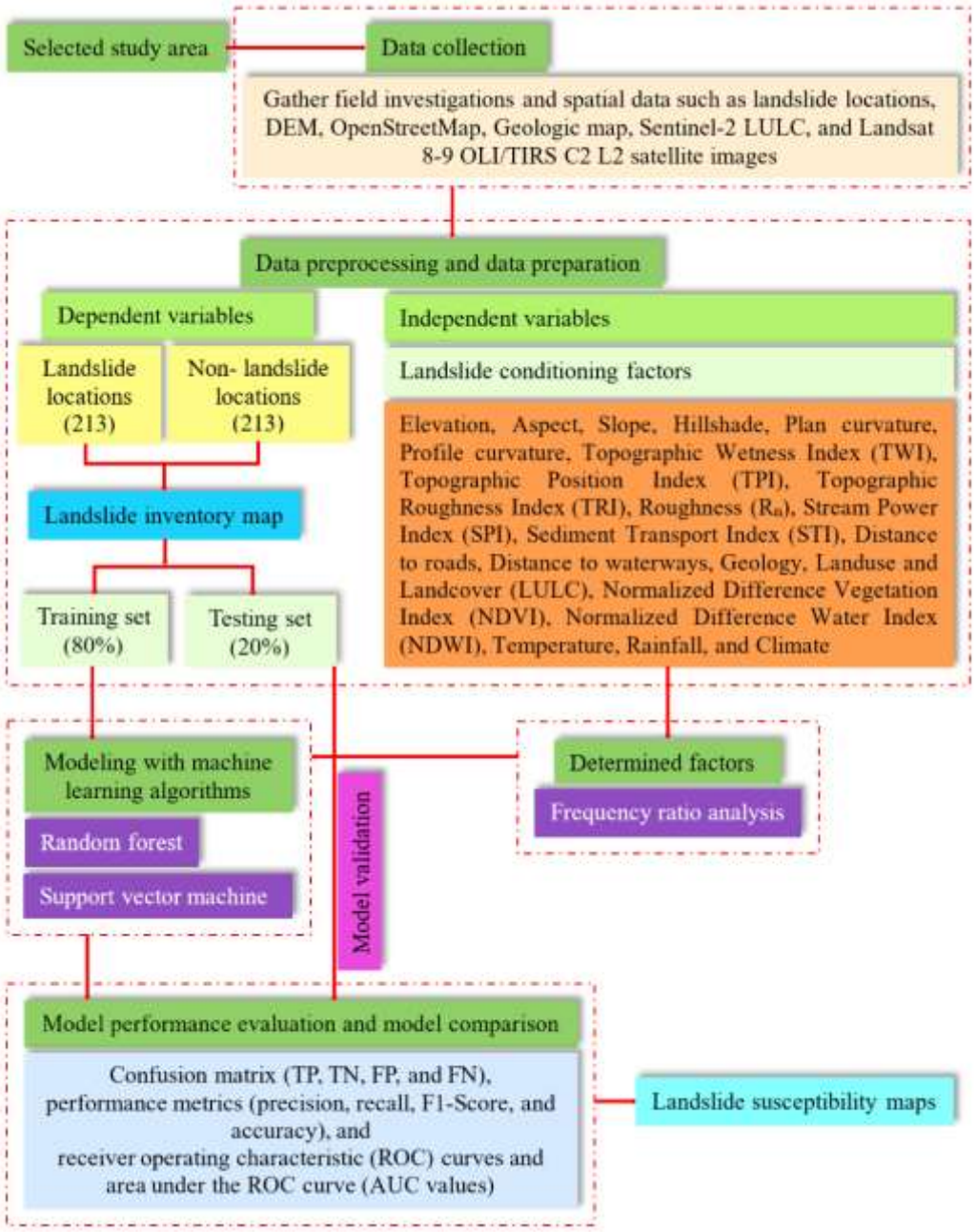

Fig. 2 Flow chart of the research methodology.

research, a total of 213 landslide locations were obtained from field investigation by the Department of Highways, Ministry of Construction and the Geological Survey and Mineral Exploration Department, Ministry of Natural Resources and Environmental Conservation in Myanmar. The landslide inventory map in this research area was generated by these field investigation data using GIS as shown in Figure 1. In the subsequent analysis to determine the likelihood of landslides occurring, an equal number of points that were not prone to landslides were randomly chosen. The dataset was then divided randomly into two sets: the training set (80 %) was used for landslide susceptibility prediction modeling, and the testing set (20 %) was used for validation of the model.

3.2. LANDSLIDE CONDITIONING FACTORS

There are currently no universally applicable guidelines when it comes to the selection of conditioning factors that contribute to the occurrence of landslides (Chen et al., 2019, 2018; Tien Bui et al., 2016). The landslide occurs due to the synergistic influence of the internal geological characteristics and external environmental elements impacting the slope (He et al., 2021; Liu et al., 2022; Nadim et al., 2006). The occurrence of landslides is influenced by the interaction of geological, morphological, topographical, and hydrological factors in a region. Thus, selecting these causal factors appropriately is a crucial initial stage in analyzing the susceptibility of landslides (Arca et al., 2019). Based on literature reviews, efficacy, and data availability, twenty-one

conditioning factors were selected and used as influencing factors for landslide susceptibility prediction modeling in this research such as elevation (m), aspect, slope (°), hillshade, plan curvature, profile curvature, topographic wetness index (TWI), topographic position index (TPI), topographic roughness index (TRI), roughness (Rn), stream power index (SPI), sediment transport index (STI), distance to roads (DTRO) (m), distance to waterways (DTWA) (m), geology, land use and land cover (LULC), normalized difference vegetation index (NDVI), normalized difference water index (NDWI), temperature (°), rainfall (mm), and climate.

Digital elevation model (DEM) is a technique used in geographic information systems (GIS) to analyze and extract information about the elevation of the Earth's surface, and that is commonly used in various scientific research (Chowdhury, 2023). A DEM with a 30 m × 30 m raster resolution was constructed from the shuttle radar topography mission digital elevation model (SRTM DEM) satellite images. The SRTM DEM data, downloaded from the United States Geological Survey (USGS) EarthExplorer website (https://earthexplorer.usgs.gov/) with a spatial resolution of 30 m, was utilized in this research. Thematic data layers related to topographic and geomorphologic factors, such as elevation, aspect, slope, hillshade, plan curvature, profile curvature, TWI, TPI, TRI, Rn, SPI, and STI were derived from the 30 m × 30 m DEM covering the research area. The remaining variables, including human-related factors (DTRO), hydrological environmental factors (rainfall, and DTWA), geological factors (geology), land cover factors (LULC, NDVI, and NDWI), and climate factors (temperature, and climate) were from the available data sourced. Subsequently, all landslides influencing factors underwent a reclassification process and were depicted as thematic maps with a consistent resolution of 30 m × 30 m.

Elevation is identified as a significant factor in evaluating landslide susceptibility in multiple studies (Guo et al., 2021; Thi Ngo et al., 2021), (Gao et al., 2022). Elevation varies across different ranges and influences soil, vegetation, rainfall, and human activities, making it a critical variable in assessing landslide risks (Gao et al., 2022; Guo et al., 2021; Thi Ngo et al., 2021). It represents the overall height of the terrain concerning the mean sea level. There is a common belief that increased elevation is associated with a higher susceptibility to landslides when contrasted with lower elevation (Ali et al., 2021; Devkota et al., 2013). In this research area, elevation was reclassified into five classes using the natural breaks (Jenks) classification method (Fig. 3a).

Aspect is a crucial topographical element influencing various microclimate variables such as rainfall intensity, soil moisture, and slope exposure, which ultimately impact the occurrence of landslides (Gao et al., 2022; Wang et al., 2019). The orientation of the slope aspect affects processes like erosion, surface evaporation, desertification, solar heating, and surface weathering, consequently influencing the frequency of landslides (Addis, 2023; Du et al., 2017; Khan et al., 2019). Aspect is a prevalent conditioning factor in conducting landslide susceptibility mapping (Pham et al., 2017; Wu et al., 2016). In the present research, the aspect is classified as flat, north, northeast, east, southeast, south, southwest, west, northwest, and north (Fig. 3b).

Slopes, in general, have a close connection to the stress field of the slope, impacting the way landslides fail and their dynamic features (Gao et al., 2022; Hong et al., 2019). In the investigation of landslide susceptibility, the slope is regarded as a significant component in the conditioning factors of slope failure (Addis, 2023; Du et al., 2017; Wang et al., 2016). As the angle of the slope increases, the probability of landslides occurring also rises (Demir et al., 2013; Roy et al., 2023). In this research, the thematic data layer of the slope angle was divided into five categories using the natural breaks (Jenks) method (Fig. 3c).

Hillshade is a technique to visualize the three-dimensional surface of a terrain by simulating light illumination from a specific angle, highlighting topographic features like hills, valleys, and slopes. Hillshade is applied to DEMs to enhance the visualization of landscapes, aiding in the interpretation of terrain characteristics and morphology. In the context of slope stability investigation, hillshade helps identify potential landslide-prone areas by emphasizing the steepness and ruggedness of the terrain through shadow effects (Rani et al., 2023). In Figure 3d, the hillshade of the research area was classified using the natural breaks (Jenks) method.

Plan curvature is formed by surfaces that intersect the horizontal plane, which affects the curvature of contour lines (Guo et al., 2021; Kormann and Lock, 2014; Rana, 2006). It influences the convergence and divergence of water flow across the surface (Liu et al., 2022). Plan curvature significantly impacts the occurrence of landslides due to its influence on the flow and accumulation of water, thereby affecting the distribution of surface moisture (Hung et al., 2016; Pham et al., 2018a). In this research, the plan curvature map is depicted in Figure 3e.

Profile curvature is the curvature of the line created by the earth's surface intersecting with the vertical plane, and its value directly represents the slope surface's geometric properties (Chen and Chen, 2021; Gao et al., 2022; Kormann and Lock, 2014; Rana, 2006). This curvature impacts the rate of acceleration and deceleration of gravitational flows downslope, stemming from the geomorphic processes of erosion and deposition that cause landslides (Kannan et al., 2013; Pal and Chowdhuri, 2019; Wang et al., 2015). In this research, the profile curvature map is shown in Figure 3f.

TWI is a critical factor influencing landslides that quantitatively represents the effect of terrain on the spatial distribution of soil moisture and is a widely utilized terrain attribute (Regmi et al., 2010). High soil

moisture content reduces soil strength, thereby increasing susceptibility to landslides. This condition is indicated by a higher TWI value, which signifies greater soil moisture content that can lead to saturation and subsequent slippage (Roy et al., 2023; Sun et al., 2020). TWI is a measure used to assess soil moisture based on DEMs (Altunel, 2023; Kopecký et al., 2021; Winzeler et al., 2022). The conditioning factor of the TWI was acquired through the utilization of a DEM with a spatial resolution of 30 meters. TWI was accomplished by applying the subsequent equation:

$$\text{TWI} = \ln\left(\frac{\text{As}}{tan\beta}\right) \quad (1)$$

In this equation, the variable As represents the specific area (m^2/m), and β represents the local slope gradient (degree) (Regmi et al., 2010). For the research area, the TWI values can be reclassified as the natural breaks (Jenks) method (Fig. 3g).

TPI illustrates the variation in elevation between a specific point and its neighboring terrain, potentially correlating with an increased risk of landslide events [64]. TPI, the position of the land surface, is determined by the difference between a cell value and the average altitude of its surrounding area. It is observed that a higher value corresponds to a greater altitude; conversely, a lower value indicates a reduced altitude. TPI results that are near 0 suggest that the terrain is either flat or on a mid-slope, while a high TPI value signifies the presence of ridges and slopes that are more susceptible to landslides (Roy et al., 2023). TPI was calculated using the following equation: (Ghasemian et al., 2022):

$$\text{TPI} = \text{Z}_0 - \sum_{n-1} Z_n/n \quad (2)$$

where Z_0 denotes the point height of the model under evaluation, Z_n represents the height of the grid, and n signifies the total number of neighboring points taken into account during the evaluation process. In this research, TPI values were reclassified into five classes using the natural breaks (Jenks) classification method (Fig. 3h).

TRI is the gradient of a topographical feature that varies spatially, which is associated with the dynamics of slope displacement (Meena et al., 2022). The TRI, a metric for assessing surface morphology, is calculated by dividing the projected area of a specific region by the total surface area of the earth (Pham et al., 2019; Roy et al., 2023). TRI is a measure of the variability or complexity of the terrain (Habib, 2021). TRI, which denotes the concave and convex upward slope, was computed according to the following equation (Althuwaynee et al., 2014).

$$\text{TRI} = \sqrt{|\text{x}|(\text{max}^2 - \text{min}^2)} \quad (3)$$

where max and min denote the highest and lowest altitude values among pixels, respectively. The TRI values of the research area can be reclassified as the natural breaks (Jenks) method (Fig. 3i).

Rn constitutes another significant landslide conditioning factor, frequently employed in various research studies to assess the susceptibility of landslides (Bostjančić et al., 2021; Das et al., 2023; Prasad et al., 2021). Rn is a measure of the variability or complexity of the terrain (Habib, 2021). Terrain heterogeneity plays a significant role in forecasting the groundwater potential within a specific region. The topographical variation in the area can be quantified through the concept of roughness. Elevated roughness values signify increased undulation, typically found in mountainous or rocky terrains, leading to heightened surface runoff and reduced water infiltration, subsequently affecting groundwater replenishment (Mukherjee and Singh, 2020). Rn was computed according to the following equation (Das et al., 2023).

$$\text{Rn} = (\text{FS}_{\text{mean}} - \text{FS}_{\text{min}}) / (\text{FS}_{\text{max}} - \text{FS}_{\text{min}}) \quad (4)$$

Where FS_{mean} represents the focal statistics mean, FS_{min} represents the focal statistics minimum and FS_{max} represents the focal statistics maximum. In this research area, the Rn values can be reclassified as the natural breaks (Jenks) method (Fig. 4j).

SPI serves as a quantification of the stream's capacity or aptitude for transporting water, thereby facilitating geomorphic processes such as channel incision, channel expansion, or aggradation. It has been observed that an elevation in slope may result in a corresponding augmentation of stream power, which could subsequently heighten the probability of landslide occurrences (Roy et al., 2023). The SPI, a variable capable of quantifying the strength and erosive potential of runoff on slope surfaces, was calculated using the subsequent equation (Poudyal et al., 2010).

$$\text{SPI} = \text{A}_\text{s} \tan\beta \quad (5)$$

Where, A_s denotes the specific catchment area (square meters), while β signifies the local slope gradient (degree). Figure 4k presents the SPI map utilized in this research.

The STI is a measure of the indicator of the erosive strength of overland flow and the subsequent sediment movement, which has the potential to compromise the stability of slopes and increase the likelihood of landslide occurrences (Ali et al., 2021). The STI indicates the extent of erosion and sediment deposition occurring in the land (Devkota et al., 2013; Lei et al., 2020). The calculation of the STI is derived from the subsequent equation:

$$\text{STI} = \left(\frac{\text{As}}{22.13}\right)^{0.6} \left(\frac{\sin\beta}{0.0896}\right)^{1.3} \quad (6)$$

Where A_s represents the specific catchment area in square meters, and sin β represents the slope gradient measured in radians (Gorsevski et al., 2016). The STI map is presented in Figure 4l of this research.

DTRO is a key factor in determining the occurrence of landslides in hilly terrain, as road construction proximity can alter the environmental

dynamics of the surrounding areas (Addis, 2023). Roads influence the incidence of landslides by disrupting the natural stability of slopes through the removal of lateral and toe support during construction activities (Dahal et al., 2008; Pham et al., 2018b). Several studies and research findings indicate that the probability of landslides decreases as the distance from roads decreases (Arabameri et al., 2019; Liu et al., 2022; Nsengiyumva et al., 2019; Paryani et al., 2020). In this research area, the maps depicting various road networks (i.e., highways, trunk, tertiary, secondary, track, service, residential, and path) were obtained from OpenStreetMap (OSM) (https://www.openstreetmap.org). The extracted features for DTRO are illustrated in Figure 4m.

In drainage networks, potential areas of slope instability can be identified due to the decrease in soil shear strength caused by elevated pore water pressure, which is a significant factor contributing to landslides (Amah et al., 2022; Chueasamat et al., 2018; Das et al., 2023; Liu et al., 2020; Rodriguez et al., 2020; Xiong et al., 2019; Zhan et al., 2019). The proximity of a slope to a river directly correlates with its likelihood of degradation, as the river's erosive power can displace and transport slope material from its initial location (Chen and Li, 2020; Yang et al., 2019). Distance to rivers and drainage is a commonly utilized distance variable in susceptibility modeling, as any element capable of introducing water into the soil within a specific area could potentially influence landslide occurrence. Water infiltration on the slope surface and within the material itself serves as the activating agent for the slope material. Drainages play a significant role in initiating various mass movements, particularly landslides, by enhancing slope instability and eroding the base of the slope material, especially in areas with steep gradients and conducive geological formations (Ashournejad et al., 2019; Bai et al., 2009; Reichenbach et al., 2018). Hence, it can be addressed that the distance from all waterways areas is a crucial variable in landslide susceptibility modeling, as proximity to water bodies significantly influences the stability of slopes. In this research area, maps depicting various waterways such as rivers, streams, weirs, canals, dams, and ditches were obtained from OSM (https://www.openstreetmap.org). The extracted features are illustrated in Figure 4n for the DTWA.

Geology plays a crucial role as the primary determinant in the occurrence of landslides, as the presence of a weak and undifferentiated lithological structure has been identified as a contributing factor leading to an escalation in landslide frequency (Neogi et al., 1998; Pal and Chowdhuri, 2019). Geological factors influencing the occurrence of landslides, such as lithology and soil type, were also included in the assessment (Pham et al., 2019; Tsangaratos and Ilia, 2016). The field of geology exerts an influence on the strength of rocks, the porosity of soil, and the permeability of materials, thereby playing a crucial role in the occurrence of landslides (Chowdhury et al., 2013; Nhu et al., 2020b). A geology map was prepared from the data set of the digital geologic layer for the map of South Asia (https://www.sciencebase.gov/). In this research area, the strata were mainly the specific distribution of various geological indexes, namely quaternary sediments (Q), paleogene sedimentary rocks (Pg), neogene sedimentary rocks (N), cretaceous sedimentary rocks (Ks), and undivided precambrian rocks (pC) (Fig. 4o).

The utilization of the earth's crust surface by humans serves a multitude of purposes. Various levels of landslide intensity are associated with different categories of land use and land cover. For instance, forests can decelerate landslides, whereas open, unproductive terrains have the potential to accelerate them. Similarly, the presence of built-up areas can also contribute to the hastening of landslides (Das and Lepcha, 2019; Roy et al., 2023). Various land cover categories exert distinct impacts on slope stability. Furthermore, alterations in land use and development can lead to the degradation of the initial vegetation cover and changes in surface water flow patterns. Consequently, this can result in the direct erosion of slopes by surface water, triggering landslides (R M and Dolui, 2021). LULC map was prepared from Sentinel-2 10 m land use/land cover time series of the world (https://www.arcgis.com). In the present research, the LULC map primarily included categories such as water, trees, flooded vegetation, crops, built areas, bare ground, clouds, and rangeland, as shown in Figure 4p.

The occurrence and spread of landslides are influenced by the presence of vegetation, primarily through the stabilizing impact of roots and stems on the incline of the terrain, which decelerates both the rate of surface water flow and the pace of water seepage (Chen and Chen, 2021). The vegetation stabilizes the soil through its root system, enhancing the soil's shear strength and playing a crucial role in mitigating landslides (Liu et al., 2022; Zhang et al., 2019). NDVI is widely recognized as a key indicator that captures the attributes of vegetation in landslide susceptibility assessment (Gigović et al., 2019; Liu et al., 2022). NDVI was extracted by Landsat 8-9 OLI/TIRS C2 L2 satellite images (https://earthexplorer.usgs.gov/) with a spatial resolution of 30 m. It is calculated based on the spectral signature of vegetation in satellite images (Singha and Swain, 2022). NDVI values range from -1 to 1, with higher values indicating healthier and denser vegetation (Gomes et al., 2019). Negative values primarily originate from clouds, water, and snow, while values close to zero are predominantly derived from rock and exposed soil. Conversely, positive values indicate the presence of vegetation coverage on the ground (Anis et al., 2019).

The NDVI is derived through the computation of reflectance values obtained from measurements in the red and near-infrared (NIR) regions of the

electromagnetic spectrum, as stated in (Chapi et al., 2017).

$$NDVI = \frac{NIR - R}{NIR + R} \quad (7)$$

Where NIR is the reflectance in the near-infrared region of the electromagnetic spectrum, and R is the reflectance in the red region of the electromagnetic spectrum. The NDVI map is depicted in Figure 4q.

NDWI is effective in detecting water bodies and assessing water content in various land cover types, which is crucial for understanding hydrological conditions that influence landslide susceptibility (Latuamury et al., 2021). NDWI was additionally derived from Landsat 8-9 OLI/TIRS C2 L2 satellite images (https://earthexplorer.usgs.gov/) with a spatial resolution of 30 m. The NDWI is affected by the moisture content of leaves, the diversity of vegetation types, and the land cover characteristics (Gao, 1996; Latuamury et al., 2021). High moisture levels in vegetation, along with an increased proportion of vegetative cover, are indicative of a high NDWI value. Conversely, low NDWI values signify a reduction in both the moisture content of the vegetation and the fraction of vegetative cover. The NDWI constitutes a transformation of the reflectance from the spectral band to extract the water's brightness level, incorporating two distinct algorithms accompanied by mathematical formulation for NDWI as below equation (Gao, 1996; Latuamury et al., 2021; Zha et al., 2003).

$$NDWI = \frac{NIR - SWIR}{NIR + SWIR} \quad (8)$$

Where NIR is the reflectance in the near-infrared region of the electromagnetic spectrum, and SWIR is the reflectance in the short-wave infrared region of the electromagnetic spectrum. Figure 4r illustrates the NDWI map.

Temperature influences landslide susceptibility by affecting slope stability through thermo-hydro-mechanical (THM) processes. Even in temperate climates, small temperature variations can significantly alter soil parameters, impacting landslide risk (Scaringi et al., 2022). The interaction between temperature and soil mechanics can alter the stability of slopes, especially those composed of clay-rich materials. This relationship is complex and involves various factors, including soil viscosity, shear strength, and hydrological conditions (Loche et al., 2022; Loche and Scaringi, 2024). Temperature data for this research was obtained from the European Centre for Medium-Range Weather Forecasts (ECMWF) Reanalysis websites (https://www.ecmwf.int/). This data was then used to generate the mean temperature map presented in Figure 5s.

Rainfall is one of the main contributors to landslides, as it can add weight to the moving mass and weaken the integrity of the rock and soil on the slope (Zhao et al., 2021). Rainfall can hasten the process of slope erosion and is consistently regarded as one of the most significant adverse influences on slope stability, particularly in mountainous and hilly regions (Liu et al., 2022; Wubalem and Meten, 2020). The intense rainfall leads to excessive saturation of the soil layer situated atop the Precambrian crystalline formations, resulting in the downhill displacement of the overburden as debris flows (Achu et al., 2023; Kuriakose et al., 2009). The rainfall data of this research were collected from the European Centre for Medium-Range Weather Forecasts (ECMWF) Reanalysis websites (https://www.ecmwf.int/) and used to generate the average monthly rainfall map for July 2024 (Fig. 5t).

Climate plays a crucial role in determining landslide susceptibility by altering rainfall patterns, increasing the frequency of extreme weather events, and affecting geological and hydrological conditions. These changes can lead to increased landslide occurrences, mainly in mountainous regions (Gunasinghe et al., 2023; Mishra et al., 2023; Saad et al., 2024; Shou, 2023; Wu, 2024). Climate changes, particularly variations in precipitation and temperature, have a significant impact on landslide occurrences (Miklin et al., 2022). The climate data for this research were acquired from the European Centre for Medium-Range Weather Forecasts (ECMWF) Reanalysis websites (https://www.ecmwf.int/). These data were then used to produce the monthly climate variable map for July 2024 presented in Figure 5u.

These twenty-one landslide conditioning factors originated from various sources; consequently, all these landslide conditioning factors maps were standardized to a uniform raster dataset format to ensure consistency and facilitate further analysis.

Moreover, to develop a more comprehensive LSMs in this research, it has been approached to incorporate monthly seasonal and climate data into the modeling process. This approach enables the creation of LSMs that more accurately reflect the dynamic nature of landslide hazards amid changing environmental conditions. By generating output maps on a month-by-month basis, it becomes possible to pinpoint critical periods where landslide risk is significantly elevated due to variations in seasonal and climate factors. Consequently, additional rainfall (mm) and climate data maps for the period of January through June 2024 have been produced for further analysis, as illustrated in Figure 6. These maps provide valuable insights into the temporal distribution of rainfall and climate patterns, offering a detailed basis across different months.

3.3. DESCRIPTION OF ANALYSIS AND MODELS

3.3.1. FREQUENCY RATIO (FR) ANALYSIS

The frequency ratio (FR) analysis is used for landslide susceptibility assessment, and it achieved the best reliability and showed a positive correlation between landslide events and landslide conditioning factors (Abdo et al., 2022). The frequency ratio of the variable can be calculated as follows (Akinci and Yavuz Ozalp, 2021):

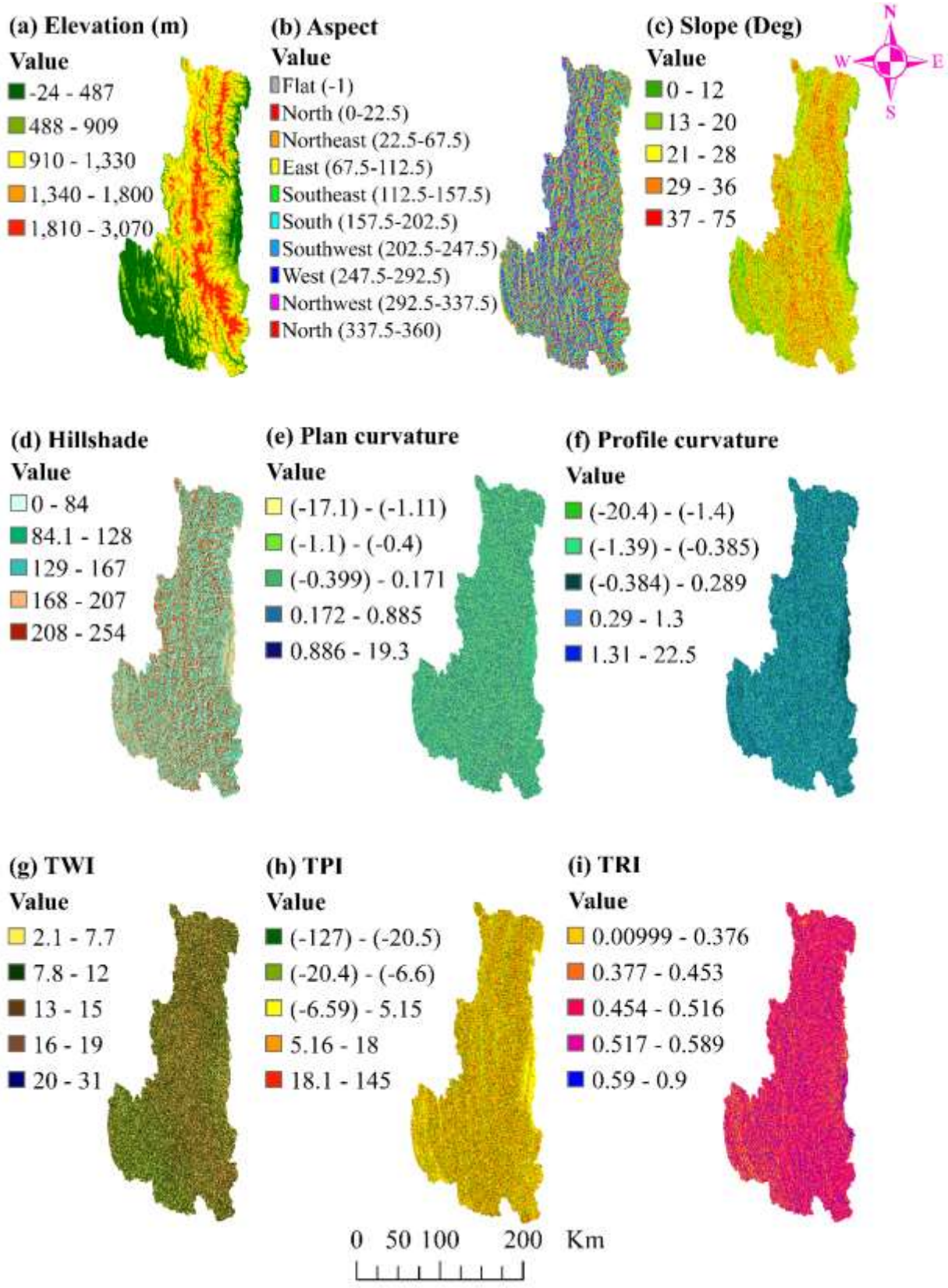

Fig. 3 Landslide conditioning factors map: (a) elevation (m), (b) aspect, (c) slope (°), (d) hillshade, (e) plan curvature, (f) profile curvature, (g) topographic wetness index (TWI), (h) topographic position index (TPI), and (i) topographic roughness index (TRI)

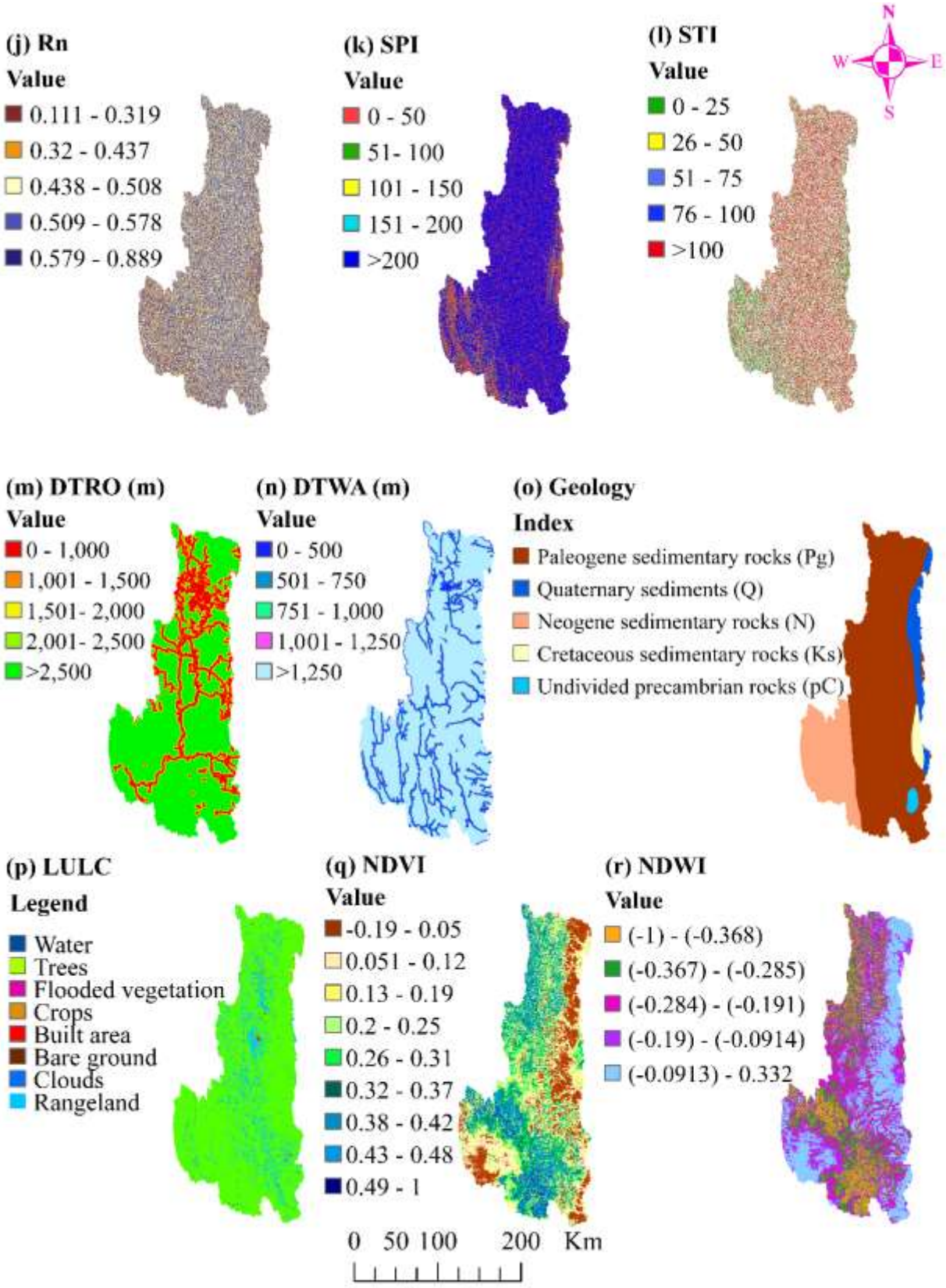

Fig. 4 Landslide conditioning factors map: (j) roughness (Rn), (k) stream power index (SPI), (l) sediment transport index (STI), (m) distance to roads (DTRO) (m), (n) distance to waterways (DTWA) (m), (o) geology, (p) land use and land cover (LULC), (q) normalized difference vegetation index (NDVI), and (r) normalized difference water index (NDWI).

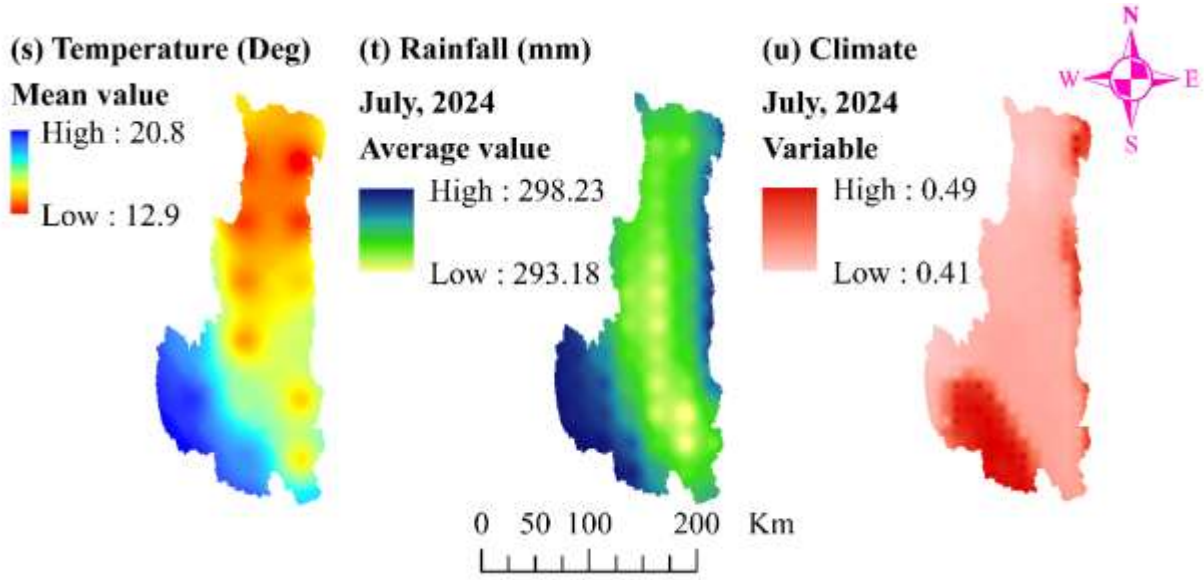

Fig. 5 Landslide conditioning factors map: (s) temperature (°), (t) rainfall (mm), (u) climate.

$$FR = \frac{(Npix\ (L_ə) - Npix\ (L_t))}{(\ Npix\ (C_ə) - Npix\ (C_t))} \quad (9)$$

Where Npix ($L_ə$) presents the number of each landslide pixel in a particular class, Npix (L_t) presents the number of total landslide pixels, Npix ($C_ə$) presents the number of pixels in a particular class, and Npix (C_t) presents the number of total pixels. The FR represents the proportion of the study area where landslides have transpired relative to each class.

3.3.2. RANDOM FOREST (RF) MODEL

RF, which was developed by Breiman (2001), is a widely utilized ensemble learning technique that has found extensive use in classification, regression, clustering, and interaction detection. RF modeling is based on bagging, a technique that combines the results of multiple decision trees trained on different samples of the dataset to reduce variations in the prediction. To create and generate a classification, RF modeling requires two parameters: the number of trees in the forest (ntree) and the number of variables tested at each node to grow the tree (mtry) (Taalab et al., 2018). Principally, it is formed by merging multiple decision trees, each of which depends on independent variables. After randomly generating several decision trees, the samples can select the best classification based on the statistical outcomes of each tree. The RF algorithm can be applied in the prediction of LSM to calculate the importance of geospatial variables (Arabameri et al., 2020) and has a significant predictive impact on the likelihood of landslide occurrences in spatial terms. The flowchart illustrating the process of the random forest is depicted in Figure 7. The RF model in this research, selection of the hyper-parameters, and construction of the landslide model were implemented using the “caret” and “randomForest” packages, respectively.

The RF model, while robust and widely used in landslide susceptibility studies, has several limitations that warrant careful consideration. One of the primary limitations is the model's potential to introduce bias due to the inherent structure of decision trees, where individual trees might favor certain variables over others depending on how the data is split (Liaw and Wiener, 2002). This can lead to overfitting, especially in cases where the model is trained on a dataset with a large number of trees, as the RF model might capture noise and small fluctuations in the data rather than generalizable patterns (Cutler et al., 2007). Although RF is generally effective in dealing with classification problems, it may struggle with imbalanced datasets, where one class significantly outweighs the other. This can lead to a model that is biased towards the majority class, potentially reducing the model's performance in predicting the minority class (Chen et al., 2004). Another critical limitation of the RF model is its lack of transparency or interpretability, often referred to as the "black box" nature of machine learning models. While RF models provide high accuracy, they do not easily offer insights into the relationships between predictors and the response variable, which can be a significant drawback in understanding the underlying mechanisms of landslide susceptibility (Breiman, 2001). This opacity can hinder the model's utility in scenarios where explainability is crucial for decision-making and policy formulation. Moreover, the model's performance is sensitive to the choice of hyperparameters, such as the number of trees and the depth of each tree, which, if not optimally selected, can compromise the model's predictive power (Biau, 2012).

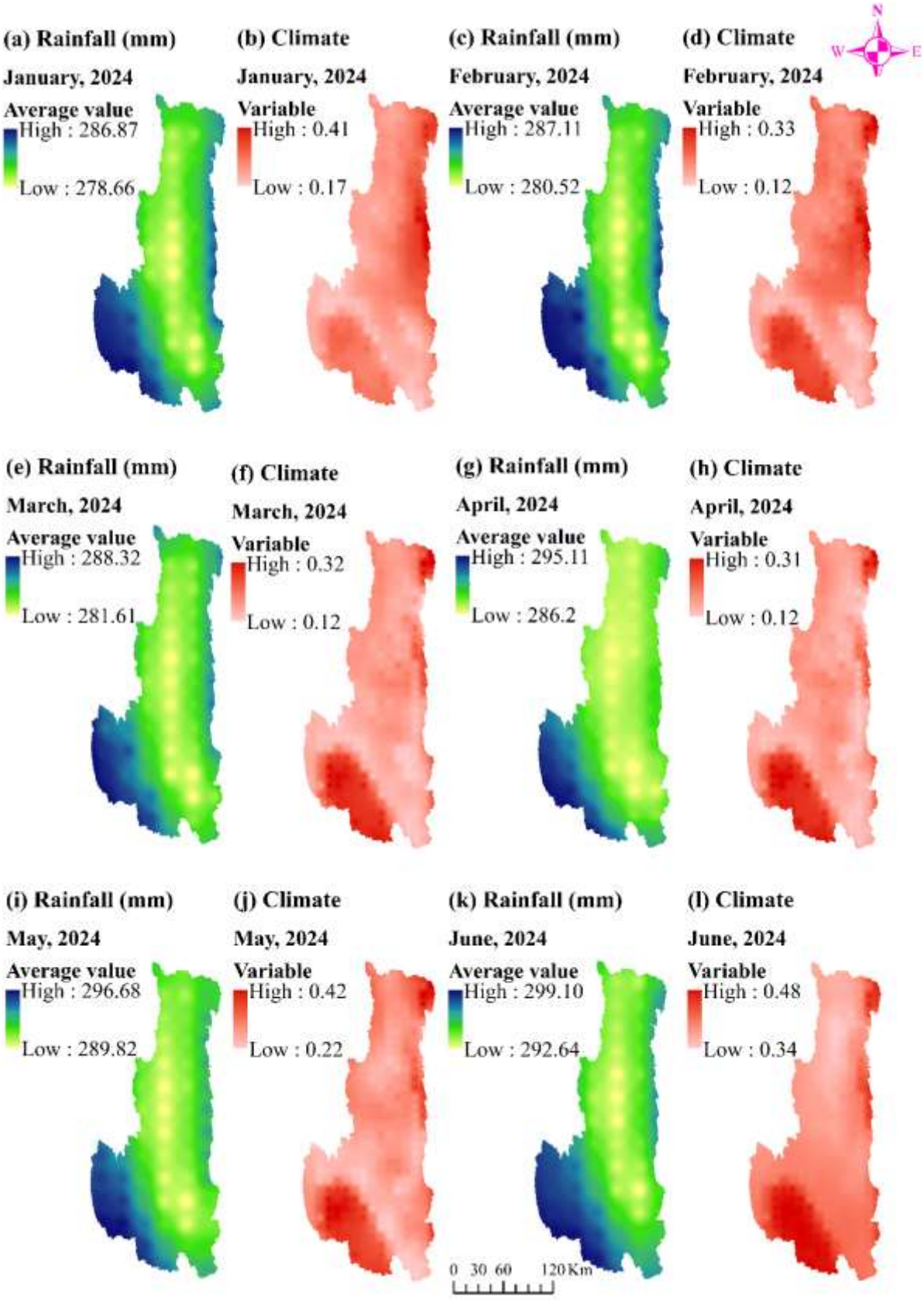

Fig. 6 Maps of average monthly rainfall data and climate data: (a) rainfall (mm) and (b) climate for January 2024; (c) rainfall (mm) and (d) climate for February 2024; (e) rainfall (mm) and (f) climate for March 2024; (g) rainfall (mm) and (h) climate for April 2024; (i) rainfall (mm) and (j) climate for May 2024; and (k) rainfall (mm) and (l) climate for June 2024.

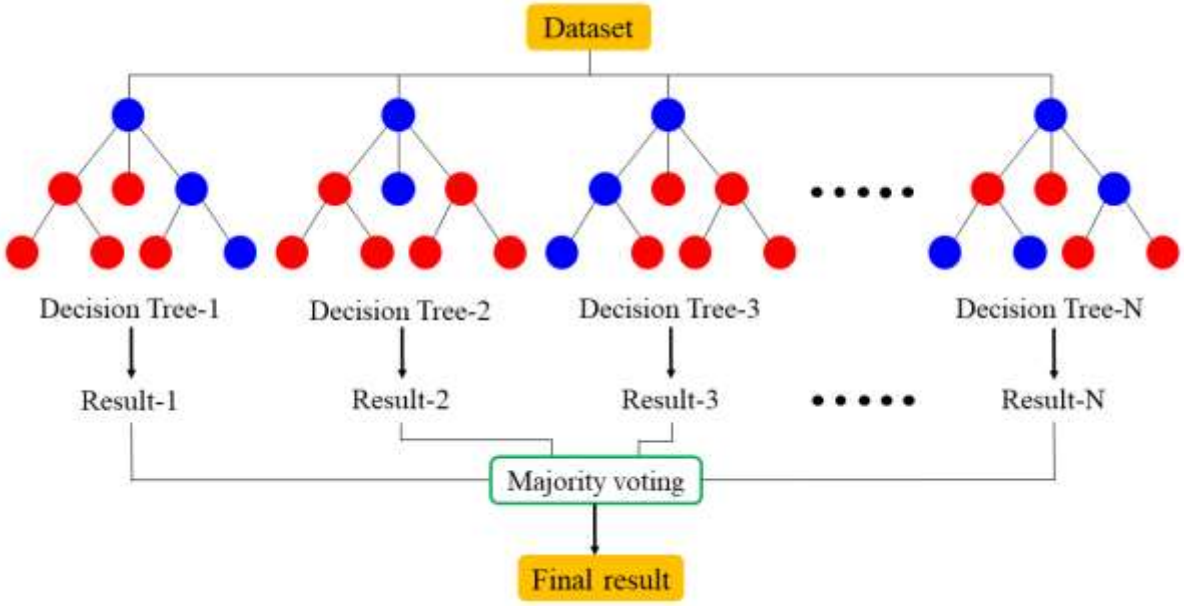

Fig. 7 Diagram depicting the flow of the RF model.

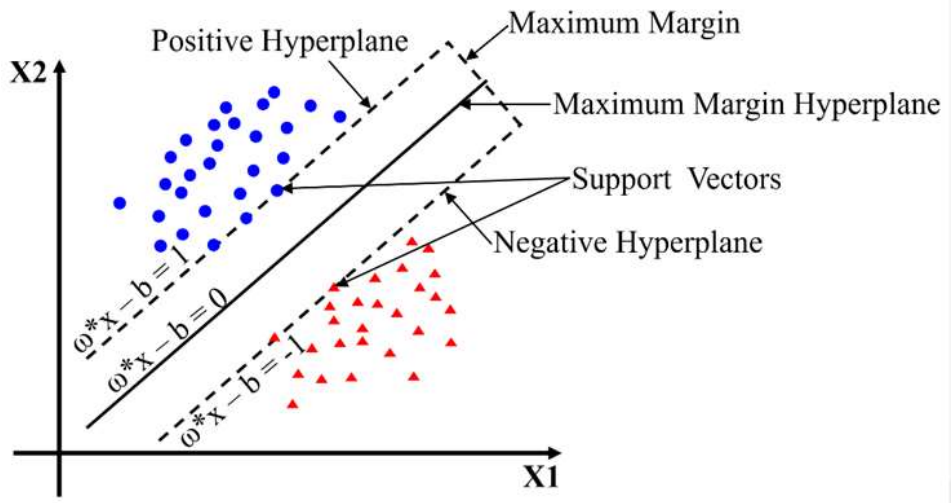

Fig. 8 Diagram depicting the SVM model for two-dimensional vectors.

3.3.3. SUPPORT VECTOR MACHINE (SVM) MODEL

SVM is a machine learning algorithm that is based on the principle of structural risk minimization from statistical learning theory, introduced by Vapnik in 1995. The SVM utilizes the landslide train dataset to accurately classify the input data into two distinct classes: landslide and non-landslide, and achieves this by mapping the data onto a feature space with a higher dimensionality and then determining an optimal hyperplane that maximizes the margin between these two classes, such as landslide and non-landslide, within a training dataset. This optimal separation is determined by the hyperplane that has the greatest distance from the nearest training dataset (Kavzoglu and Colkesen, 2009; Pham et al., 2018b; Samui, 2008). To achieve linear classification, a kernel function is used to transform the non-linear data into a higher-dimensional feature space. There are different types of kernel functions, such as linear, polynomial, radial, and sigmoid (Dou et al., 2019; Pourghasemi and Kerle, 2016). The optimum hyperplane is generated through the decision function $f(x) = (\omega. \emptyset(x)) - b$, where ω denotes the coefficient vector that specifies the orientation of the classification hyperplane, $\emptyset(x)$ represents the input sample x transformed into the high-dimensional feature space, and b denotes the offset of the hyperplane obtained from the origin. The operational principles and decision-making process of the SVM algorithm within a feature space are illustrated, as shown in Figure 8. In this research SVM model, the "e1071" package was used and the specified method "svmRadial" to construct the landslide model.

The SVM models are powerful tools for classification and regression tasks, including landslide susceptibility prediction modeling. However, one of

Table 1 Confusion matrix

Confusion Matrix		Actual Condition	
		Positive	**Negative**
Predicted Condition	**Positive**	True Positive (TP)	False Positive (FP)
	Negative	False Negative (FN)	True Negative (TN)

the main limitations of SVMs is their sensitivity to the choice of kernel and hyperparameters. The performance of an SVM model heavily relies on selecting the appropriate kernel function (e.g., linear, polynomial, radial basis function, and sigmoid) and fine-tuning the associated hyperparameters such as the regularization parameter (C) and kernel-specific parameters (e.g., gamma in the radial basis function) (Hsu et al., 2016). Improper selection of these parameters can lead to either overfitting or underfitting, where the model either captures too much noise or fails to capture the underlying patterns in the data, respectively. Another significant limitation of SVM models is their computational complexity, especially in the presence of large datasets with high-dimensional features (Christmann and Steinwart, 2008). The SVM models also assume that the data is linearly separable in the transformed feature space, which may not always be the case in complex environmental datasets. Although kernel functions help in mapping the data to a higher-dimensional space where it may become linearly separable, this approach can introduce additional uncertainties related to the choice of kernel and the risk of overfitting (Cristianini and Shawe-Taylor, 2000). Furthermore, the SVMs do not inherently provide probabilistic outputs, which can be a limitation when the goal is to estimate the likelihood of events, such as the probability of a landslide occurrence (Platt, 2000).

3.4. MODEL PERFORMANCE EVALUATION

3.4.1. CONFUSION MATRIX AND PERFORMANCE METRICS

For model performance evaluation, it can be used performance metrics such as accuracy, precision, recall, and F1-Score (Botchkarev, 2019; Ferri et al., 2009; Hand, 2012). The visualization of algorithm performance is facilitated by the confusion matrix, which is a tabular arrangement. Each row represents instances predicted under a specific condition, while each column represents instances observed under an actual condition, as exemplified in Table 1 (Azarafza et al., 2022; Muller and Guido, 2016). The confusion matrix, which incorporates metrics like accuracy, precision, recall, and F1-Score, functions as a structured display illustrating the performance of a predictive model. In classification scenarios, the evaluation of the classifier's performance against established benchmarks relies heavily on true positive (TP), true negative (TN), false positive (FP), and false negative (FN) (Muller and Guido, 2016).

The impact of this matrix on predictive analytics is positive as it clearly defines true positives (instances where the model accurately predicts the positive class), true negatives (instances where the model accurately predicts the negative class), false positives (instances where the model inaccurately predicts the positive class), and false negatives (instances where the model inaccurately predicts the negative class). The utilization of the confusion matrix is aimed at quantifying the precise ratio of correct classifications, thus acting as a measure of the effectiveness of the predictive model, especially in scenarios involving imbalanced training-testing datasets, which might lead to inaccurate assessments of accuracy. Additionally, this matrix functions as a valuable information source concerning the precision, recall (sensitivity), F1-Score, and accuracy of the predictive model, as illustrated in the subsequent equations (Aggarwal, 2023; Azarafza et al., 2022).

$$\text{Precision} = \frac{\text{True Positive (TP)}}{\text{True Positive (TP)} + \text{False Positive (FP)}} \tag{10}$$

$$\text{Recall} = \frac{\text{True Positive (TP)}}{\text{True Positive (TP)} + \text{False Negative (FN)}} \tag{11}$$

Then again, the F1-Score, identified as the harmonic average of precision and recall, provides an estimation of the midpoint between the two values in close proximity and commonly signifies the harmonic mean more extensively (Aggarwal, 2023; Azarafza et al., 2022).

$$\text{F1-Score} = 2 \cdot \frac{\text{Precision} \cdot \text{Recall}}{\text{Precision} + \text{Recall}} \tag{12}$$

Full precision indicates the probability that a person will be accurately classified by a test; precisely, the sum of true positives plus true negatives divided by the total number of individuals assessed (Aggarwal, 2023; Azarafza et al., 2022).

$$\text{Accuracy} = \frac{\text{True Positive (TP)} + \text{True Negative (TN)}}{\text{True Positive (TP)} + \text{True Negative (TN)} + \text{False Positive (FP)} + \text{False Negative (FN)}} \tag{13}$$

3.4.2. RECEIVER OPERATING CHARACTERISTIC (ROC) CURVES AND AREA UNDER THE ROC CURVE (AUC VALUES)

ROC curves use true positive rate (TPR) and false positive rate (FPR) to summarize classification performance. TPR is the proportion of positive examples predicted correctly (recall). FPR is the proportion of negative examples predicted incorrectly. The TPR and the FPR are defined as follows:

$$\text{TPR} = \frac{\text{True Positive (TP)}}{\text{True Positive (TP)} + \text{False Negative (FN)}} \quad (14)$$

$$\text{FPR} = \frac{\text{False Positive (FP)}}{\text{False Positive (FP)} + \text{True Negative (TN)}} \quad (15)$$

ROC curves are employed to evaluate classifiers that provide a confidence score or probability of prediction. The confidence score range is discretized to create the ROC curve, for example, into intervals like [0, 0.1, 0.2..., 1]. Each discrete value in the range is used as the prediction threshold, and the labels of examples are predicted accordingly. TPR and FPR are computed for each threshold. The higher the area under the ROC curve (AUC), the better the classifier performs. A classifier with an AUC greater than 0.5 outperforms a random classifier. If the AUC is < 0.5, there are issues with the model. An ideal classifier would have an AUC of 1. Typically, a good classifier is achieved by selecting a threshold value that yields a TPR close to 1 while maintaining an FPR near 0. ROC curves are widely utilized because they are relatively easy to comprehend and encompass multiple aspects of classification by considering both false positives and false negatives (Burkov, 2019).

4. RESULTS AND DISCUSSION

4.1. FREQUENCY RATIO OF THE LANDSLIDE OCCURRENCE IN EACH CLASS OF THE LANDSLIDE CONDITIONING FACTORS

FR analysis is a widely used statistical method for evaluating the relationship between landslide conditioning factors and landslide occurrences. This approach quantifies the degree of association between various factor classes and the presence of landslides, offering a robust framework for understanding the influence of each conditioning factor on landslide susceptibility. Each factor was classified into several classes, and the FR for each class was calculated. This process helps to identify which factor classes are more conducive to landslide occurrences. The FR was normalized to a range of 0 to 1, with the highest frequency of landslides showing 1 and the lowest frequency near 0. This normalized frequency ratio (FR_n) supports clarifying the spatial relationship between landslide conditioning factors and occurrence.

The analysis of elevation revealed distinct ranges associated with varying frequencies of landslide occurrence, indicating notable differences in susceptibility across different elevation intervals. Specifically, within the elevation range of 1,810 to 3,070 meters, the highest frequency of landslides was observed, corresponding to a FR_n value of 1. This suggests a significant correlation between high elevations and landslide susceptibility within the study area. Typically, higher elevations are associated with steeper slopes, which inherently possess greater gravitational force acting on the slope materials, increasing the likelihood of landslide occurrences. In terms of aspect, areas facing the Southeast exhibited the highest susceptibility, with FR_n value of 1, indicating the highest proportion of landslide occurrence. Concerning the slope, slopes ranging from 37° to 75° exhibit the highest susceptibility in this area, as indicated by the FR_n value of 1, suggesting the highest likelihood of landslide occurrence in this gradient range. Conversely, areas with slopes between 0° and 12° demonstrate the lowest susceptibility, with an FR_n value of 0.72, implying a reduced probability of landslide incidents in such terrain conditions. Areas with hillshade values ranging from 0 to 84 exhibit the highest susceptibility, as indicated by an FR_n value of 1, suggesting a significantly elevated likelihood of landslide occurrence in regions with lower illumination. Conversely, terrain with hillshade other values, that is, 84.1 - 128, 129 - 167, 168 - 207, and 208 - 254 have FR_n values of 0.98, 0.70, 0.57, and 0.17, respectively. Plan curvature values between 0.172 and 0.885 display the highest susceptibility, as specified by the FR_n value of 1, suggesting an elevated likelihood of landslide occurrence in areas with concave landforms. Profile curvature values between - 1.39 and -0.385 exhibit the highest susceptibility to landslides, with FR_n of 1, suggesting a significant probability of landslide occurrence. This area typically represents concave landforms, where terrain curvature contributes to water and sediment accumulation, increasing the risk of slope instability. The analysis of TWI reveals varying levels of landslide susceptibility across different TWI ranges. The TWI values between 20 and 31 exhibit the highest susceptibility to landslides, through FR_n of 1, indicating a significant probability of landslide occurrence. This area typically corresponds to areas with high moisture content and low drainage capacity, making them prone to slope instability. The TPI values (5.16 - 18) classes, through FR_n of 1, show a higher likelihood of landslide occurrence, indicating that areas with higher topographic positions, such as ridges or hills, are more prone to landslides. The higher class with TRI values (0.59 - 0.9) has the highest FR_n values of 1, suggesting a strong association with landslide occurrence. The analysis of Rn indicates varying levels of landslide susceptibility across different ranges of roughness values. The roughness values between 0.442 - 0.508, 0.509 - 0.578, and 0.579 - 0.889 exhibit a higher susceptibility to landslides and show higher FR_n values, suggesting a significant probability of landslide occurrence in this area. This area typically represents areas with rugged terrain and irregular surface characteristics, which contribute to slope instability and increased landslide risk. The classes

with higher SPI values (>200) and STI values (>100) demonstrate the strongest correlation with landslide occurrences, as indicated by their maximum FR_n values of 1. This suggests that areas with elevated SPI and STI values are particularly vulnerable to landslides. High SPI values reflect regions where water flow has sufficient energy to erode and transport sediment, thereby destabilizing slopes. In these areas, the force exerted by the flowing water is substantial, leading to increased erosion and a higher probability of landslide events. Similarly, high STI values indicate regions where the potential for sediment movement is significant. In areas with elevated STI, the capacity for sediment to be detached and transported by water or other means is greater, making these regions more susceptible to landslides. The strong association between high STI values and landslide occurrence underscores the critical role of sediment transport processes in destabilizing slopes and triggering landslides. For DTRO, areas categorized within 0 to 1000 meters from roads exhibited the highest FR_n value of 1. This indicates a strong correlation between proximity to roads and the likelihood of landslide occurrence. The FR_n value diminishes progressively as the distance from roads increases, suggesting that landslide susceptibility decreases in areas farther from roads. This pattern could be attributed to the fact that road construction and associated activities often destabilize slopes, leading to higher landslide risks in nearby areas. For DTWA, the category of 0 to 500 meters from waterways also showed the highest FR_n value of 1. This implies that areas close to water bodies are more prone to landslides, likely due to the effects of water erosion, saturation of soils, and potential undercutting of slopes by flowing water. Such characteristics make these regions more susceptible to landslide events, especially during periods of heavy rainfall or increased water flow. The analysis of the relationship between landslides and geological formations reveals that landslides are most likely to occur in areas dominated by Paleogene sedimentary rocks (Pg), as indicated by the highest FR_n value of 1. This suggests that the specific characteristics of these sedimentary rocks, such as their composition, weathering patterns, and structural weaknesses, contribute significantly to the susceptibility of these areas to landslides. The presence of these rocks may create conditions that facilitate slope instability, leading to a higher frequency of landslide occurrences. The analysis of LULC factors highlights varying levels of landslide susceptibility across different land cover types. Among these, areas classified as "built areas" demonstrate the highest susceptibility to landslides, with the FR_n value of 1. This elevated risk can be attributed to several factors. Urban and built-up areas often involve significant modifications to the natural landscape, such as excavation, construction, and deforestation, which can lead to increased soil erosion and reduced stability of the ground. The lack of natural vegetation in these areas further exacerbates the problem, as vegetation typically plays a crucial role in stabilizing soil and preventing erosion. The results indicate an unusual pattern where the highest ranges of NDVI values, between 0.4 and 1, and the highest NDWI values, ranging from -0.0913 to 0.332, correspond to the highest susceptibility to landslides, as indicated by an FR_n value of 1. This outcome is intriguing, as high NDVI values typically represent areas with dense vegetation, which is generally associated with greater slope stability due to the root systems of plants that help anchor the soil. Similarly, positive NDWI values usually indicate the presence of water bodies or moisture-rich areas, which might also contribute to soil stability. However, in this study area, the highest values of NDVI and NDWI correlate with increased landslide susceptibility. This abnormal result could be explained by the possibility that areas with high vegetation density might also experience higher rainfall interception, leading to increased soil moisture and a higher likelihood of landslides when the soil becomes saturated. Additionally, high NDWI values might indicate regions with excessive moisture, which could lead to soil saturation and reduced cohesion, thereby increasing the risk of landslides. Additionally, these areas may experience more significant pore water pressure, further destabilizing the slopes. Classes with temperature ranges between 14.8 and 15.9 exhibit the highest FR_n values of 1, indicating that this temperature range is particularly conducive to conditions that trigger landslides. This could be related to the fact that these temperatures may influence the freezing and thawing cycles in the soil, increasing susceptibility to landslides. Rainfall classes within the range of 293.18 to 294.51 mm show higher FR_n values, which aligns with the understanding that increased rainfall directly contributes to landslide occurrences by elevating pore water pressure in the soil, reducing its shear strength, and triggering slope failures. Furthermore, the analysis shows that moderate climate values, particularly in the range of 0.42 to 0.43, also correspond to higher FR_n values. This suggests that these climatic conditions, which may involve a particular combination of temperature, humidity, and precipitation patterns, create an environment where landslides are more likely to occur. The FR analysis quantifies factors influencing landslide susceptibility, aiding in accurate modeling and prioritizing significant influences, enhancing understanding of underlying mechanisms driving landslides in this study area. The results of the FR analysis of each factor are summarized in Table 2.

4.2. LANDSLIDE SUSCEPTIBILITY MAPS GENERATED BY THE RF MODEL AND SVM MODELS

The LSMs obtained from the RF and SVM models demonstrated a discernible susceptibility level from very low to very high, underscoring their efficacy in predicting landslide occurrences. The LSM generated by the RF model was classified into five susceptibility categories: very low (0 - 0.108), low

Table 2 The spatial relationship between each landslide conditioning factor and landslide occurrence by FR analysis.

Factors	Classes	No. of Class pixels	No. of Landslide pixels	Frequency Ratio	Normalized Frequency Ratio (FR_n)
Elevation (m)	-24 – 487	9102396	9900	0.229	0.07
	488 – 909	9204526	12600	0.288	0.09
	910 - 1,330	9949605	33300	0.705	0.22
	1,340 - 1,800	7827886	73800	1.985	0.61
	1,810 - 3,070	3907260	60300	3.250	1.00
Aspect	Flat (-1)	3951619	18000	0.958	0.52
	North (0 - 22.5)	3898812	25200	1.360	0.74
	Northeast (22.5 - 67.5)	4090960	12600	0.648	0.35
	East (67.5 - 112.5)	4219734	26100	1.301	0.71
	Southeast (112.5 - 157.5)	4016456	35100	1.838	1.00
	South (157.5 - 202.5)	4128011	35100	1.789	0.97
	Southwest (202.5 - 247.5)	4067086	18000	0.931	0.51
	West (247.5 - 292.5)	3839926	7200	0.394	0.21
	Northwest (292.5 - 337.5)	3669429	4500	0.258	0.14
	North (337.5 - 360)	4066104	8100	0.419	0.23
Slope (°)	0 - 12	5418766	22500	0.873	0.72
	13 - 20	9774151	46800	1.007	0.83
	21 - 28	11686200	62100	1.118	0.92
	29 - 36	9346450	36900	0.831	0.68
	37 - 75	3722570	21600	1.221	1.00
Hillshade	0 - 84	3614550	27900	1.623	1.00
	84.1 - 128	7288807	54900	1.584	0.98
	129 - 167	8801796	47700	1.140	0.70
	168 - 207	10563839	46800	0.932	0.57
	208 - 254	9666146	12600	0.274	0.17
Plan curvature	(-17.1) - (-1.11)	1630835	7200	0.930	0.86
	(-1.1) - (-0.4)	6476191	31500	1.024	0.95
	(-0.399) - 0.171	14613203	64800	0.934	0.87
	0.172 - 0.885	13397741	68400	1.075	1.00
	0.886 - 19.3	3873991	18000	0.979	0.91
Profile curvature	(-20.4) - (-1.4)	857561	3600	0.884	0.80
	(-1.39) - (-0.385)	5125163	27000	1.109	1.00
	(-0.384) - 0.289	15136987	76500	1.064	0.96
	0.29 - 1.3	16175052	72900	0.949	0.86
	1.31 - 22.5	2697198	9900	0.773	0.70
TWI	2.1 - 7.7	2793340	11700	0.887	0.70
	7.8 - 12	8091323	24300	0.636	0.50
	13 - 15	13281487	70200	1.120	0.88
	16 - 19	11550670	56700	1.040	0.82
	20 - 31	4513308	27000	1.267	1.00
TPI	(-127) - (-20.5)	3513361	4500	0.270	0.22
	(-20.4) - (-6.6)	9099934	37800	0.875	0.71
	(-6.59) - 5.15	12228223	63900	1.100	0.89
	5.16 - 18	9977529	58500	1.235	1.00
	18.1 - 145	5172626	25200	1.026	0.83

Table 2 (continued)

Factors	Classes	No. of Class pixels	No. of Landslide pixels	Frequency Ratio	Normalized Frequency Ratio (FR_n)
TRI	0.00999 - 0.376	2792623	10800	0.815	0.72
	0.377 - 0.453	8087170	24300	0.634	0.56
	0.454 - 0.516	13284406	70200	1.114	0.98
	0.517 - 0.589	11550979	61200	1.117	0.98
	0.59 - 0.9	4513678	24300	1.135	1.00
Rn	0.111 - 0.322	1112063	1800	0.340	0.32
	0.323 - 0.441	5991527	27000	0.947	0.89
	0.442 - 0.508	14934222	72000	1.013	0.96
	0.509 - 0.578	13203289	66600	1.060	1.00
	0.579 - 0.889	4476092	21600	1.014	0.96
SPI	0 - 50	2017	0.000	0.000	0.00
	51 - 100	2557	0.000	0.000	0.00
	101 - 150	6337	0.000	0.000	0.00
	151 - 200	24901	0.000	0.000	0.00
	>200	39912710	189900	1.001	1.00
STI	0 - 25	2069	0.000	0.000	0.00
	26 - 50	5031	0.000	0.000	0.00
	51 - 75	14034	0.000	0.000	0.00
	76 - 100	50241	0.000	0.000	0.00
	>100	20264550	102600	1.004	1.00
DTRO (m)	0 - 1000	17695868	167400	1.992	1.00
	1001 - 1500	10892881	15300	0.102	0.04
	1501 - 2000	5924701	1800	0.019	0.01
	2001- 2500	3586027	1800	0.021	0.01
	>2500	1892484	3600	0.047	0.03
DTWA (m)	0 - 500	13852099	64800	0.985	1.00
	501 - 750	11852529	43200	0.768	0.67
	751 - 1000	8110448	45900	1.192	0.71
	1001- 1250	4679319	18000	0.810	0.28
	>1250	1498032	18000	2.530	0.28
Geology	Paleogene sedimentary rocks (Pg)	28709029	172800	1.268	1.00
	Quaternary sediments (Q)	2428058	8100	0.703	0.55
	Neogene sedimentary rocks (N)	7722012	8100	0.221	0.17
	Cretaceous sedimentary rocks (Ks)	760013	0.000	0.000	0.00
	Undivided Precambrian rocks (pC)	373694	900	0.507	0.40
LULC	Water	134799	0.000	0.000	0.00
	Trees	34610794	72900	0.442	0.02
	Flooded vegetation	170	0.000	0.000	0.00
	Crops	62376	0.00	0.000	0.00
	Built area	155407	16200	21.851	1.00
	Bare ground	6974	0.000	0.000	0.00
	Clouds	163	0.000	0.000	0.00
	Rangeland	5024259	101700	4.243	0.19

Table 2 (continued)

Factors	Classes	No. of Class pixels	No. of Landslide pixels	Frequency Ratio	Normalized Frequency Ratio (FR_n)
NDVI	-0.19 - 0.092	11566298	7200	0.130	0.04
	0.093 - 0.2	7604440	18000	0.496	0.16
	0.21 - 0.3	8339700	49500	1.244	0.41
	0.31 - 0.39	7493257	44100	1.234	0.41
	0.4 - 1	4989232	72000	3.025	1.00
NDWI	(-1) - (-0.368)	4435303	7200	0.340	0.26
	(-0.367) - (-0.285)	7636923	18000	0.494	0.38
	(-0.284) - (-0.191)	8984480	49500	1.155	0.90
	(-0.19) - (-0.0914)	7204810	44100	1.283	0.99
	(-0.0913) - 0.332	11730304	72000	1.287	1.00
Temperature	12.9 - 14.7	8400147	50400	1.264	0.55
	14.8 - 15.9	9746229	107100	2.314	1.00
	16 - 17.4	9560659	20700	0.456	0.20
	17.5 - 19	4732124	3600	0.160	0.07
	19.1 - 20.8	7552455	8100	0.226	0.10
Rainfall (mm)	293.18 - 294.51	6582212	77400	2.476	1.00
	294.52 - 295.18	10828062	46800	0.910	0.37
	295.19 - 295.99	8694504	43200	1.046	0.42
	296.00 - 297.02	6499368	18000	0.583	0.24
	297.03 - 298.23	7387473	4500	0.128	0.05
Climate	0.41 - 0.42	9887274	41400	0.886	0.58
	0.42 - 0.43	19246796	139500	1.534	1.00
	0.44 - 0.45	3172780	3600	0.240	0.16
	0.46 - 0.47	2506895	1800	0.152	0.10
	0.48 - 0.49	5178367	2700	0.110	0.07

(0.109 - 0.159), moderate (0.16 - 0.267), high (0.268 - 0.5), and very high (0.501 - 1), as shown in Figure 9a and summarized in Table 3. Subsequent analysis revealed that the portion of the area covered in the very low susceptibility is 22.98 % of the total study area, while the portion of the area covered in the very high susceptibility is 13.98 %, with low, moderate, and high susceptibility areas accounting for 13.21 %, 23.47 %, and 26.36 % of the total area, respectively (Table 3). The proportion of landslides occurring within each susceptibility class was determined, revealing that 0.94 %, 0.47 %, 1.42 %, 9.43 %, and 87.74 % of landslides transpired in the very low, low, moderate, high, and very high susceptibility classes, respectively (Table 3). Then, the LSM was derived from the SVM model, and this LSM was reclassified into five susceptibility classes, namely, very low, low, moderate, high, and very high susceptibility categories. These susceptibility classifications were defined by ranges of susceptibility values: very low (0.00164 - 0.0961), low (0.0962 - 0.226), moderate (0.227 - 0.403), high (0.404 - 0.646), and very high (0.647 - 0.979), as described in Figure 9b and summarized in Table 3. Subsequently, the distribution of these percentages across the susceptibility classes revealed in the SVM model, the proportions of area coverage in the very low, low, moderate, high, and very high susceptibility levels were 18.37 %, 18.62 %, 22.13 %, 26.24 %, and 14.64 %, respectively (Table 3). The percentage of landslide coverage within each class was determined, indicating that 3.79 %, 3.32 %, 6.16 %, 24.64 %, and 62.09 % of landslides occurred in the very low, low, moderate, high, and very high susceptibility classes, respectively (Table 3). The RF and SVM models observed that areas characterized by high and very high susceptibility were predominantly concentrated in the northern and northeastern parts of the state, suggesting localized susceptibility to landslide occurrences in mostly surrounding the areas of Hakka and Falam. Field studies conducted by researchers (Yasukuni and Soe, 2017) have reported the conditions of landslide occurrences in Hakka and its environs, as well as the northern areas of Chin State. Additionally, findings from previous research studies (Kyaw Htun et al., 2019) have highlighted the susceptibility of these regions to landslides due to factors such as geological complexity, rugged terrain, and heavy rainfall by field observation. The same

Table 3 Features of five susceptibility levels in LSMs by the RF and SVM models.

	RF model				SVM model			
Susceptibility levels	Classes	Area covered %	Landslides covered %	Landslide density	Classes	Area covered %	Landslides covered %	Landslide density
Very low	0 - 0.108	22.98	0.94	0.041	0.00164 - 0.0961	18.37	3.79	0.206
Low	0.109 - 0.159	13.21	0.47	0.036	0.0962 - 0.226	18.62	3.32	0.178
Moderate	0.16 - 0.267	23.47	1.42	0.060	0.227 - 0.403	22.13	6.16	0.278
High	0.268 - 0.5	26.36	9.43	0.358	0.404 - 0.646	26.24	24.64	0.939
Very high	0.501 – 1	13.98	87.74	6.277	0.647 - 0.979	14.64	62.09	4.240
Total		100	100	6.772		100	100	5.842

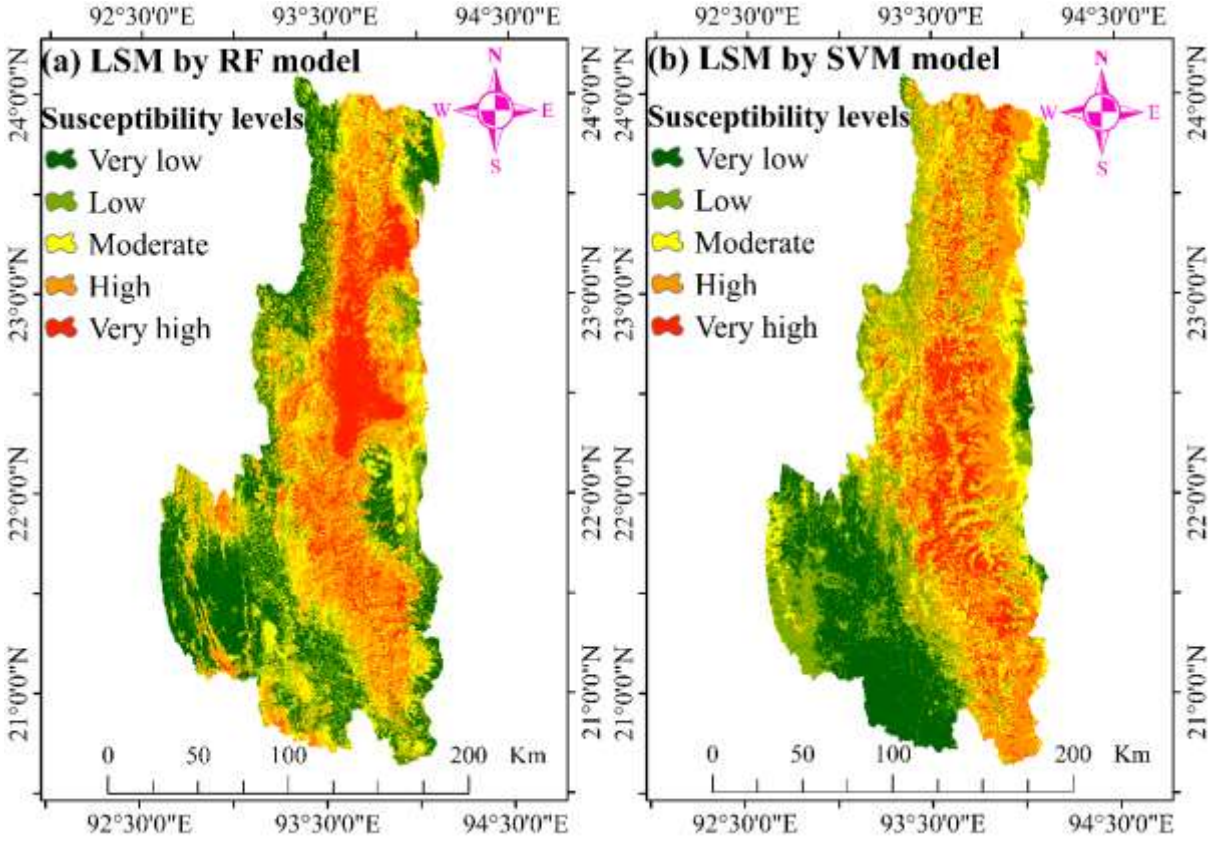

Fig. 9 Landslide susceptibility maps: (a) RF model and (b) SVM model.

between the model predictions and field observations reinforces the reliability of the RF and SVM machine learning models for LSM in Chin State. Moreover, specified the model predictions with FR_n values from FR analysis, the concentration of high and very high susceptibility to landslides in the northern and northeastern parts of Chin State can be attributed to a combination of factors related to this area's terrain, geology, and environmental characteristics. LSMs generated for the study area indicate that regions with high and very high susceptibility are predominantly concentrated in the highest elevation zones. This observation aligns well with the findings from the FR analysis, where the highest elevation range (1,810 to 3,070 m) was associated with the highest FR_n value of 1, signifying a strong correlation between high elevations and landslide occurrences. The highest elevation class not only demonstrated a high frequency of landslides but also showed a consistent pattern of susceptibility across the maps. Also, the slopes ranging from 37° to 75° and the Paleogene sedimentary rocks (Pg) geology area indicated high and very high landslide occurrence zones in the maps; this observation also aligns well with the findings from the FR analysis, shown by the highest FR_n value of 1. These combination factors collectively create conditions conducive to landslide occurrences in these areas of high susceptibility.

Based on the LSMs generated from the RF and SVM models, the landslide density for each susceptibility class on the LSMs can be computed. Landslide density is defined as the ratio of the percentage of landslides covered to the percentage of area covered on each susceptibility class displayed on

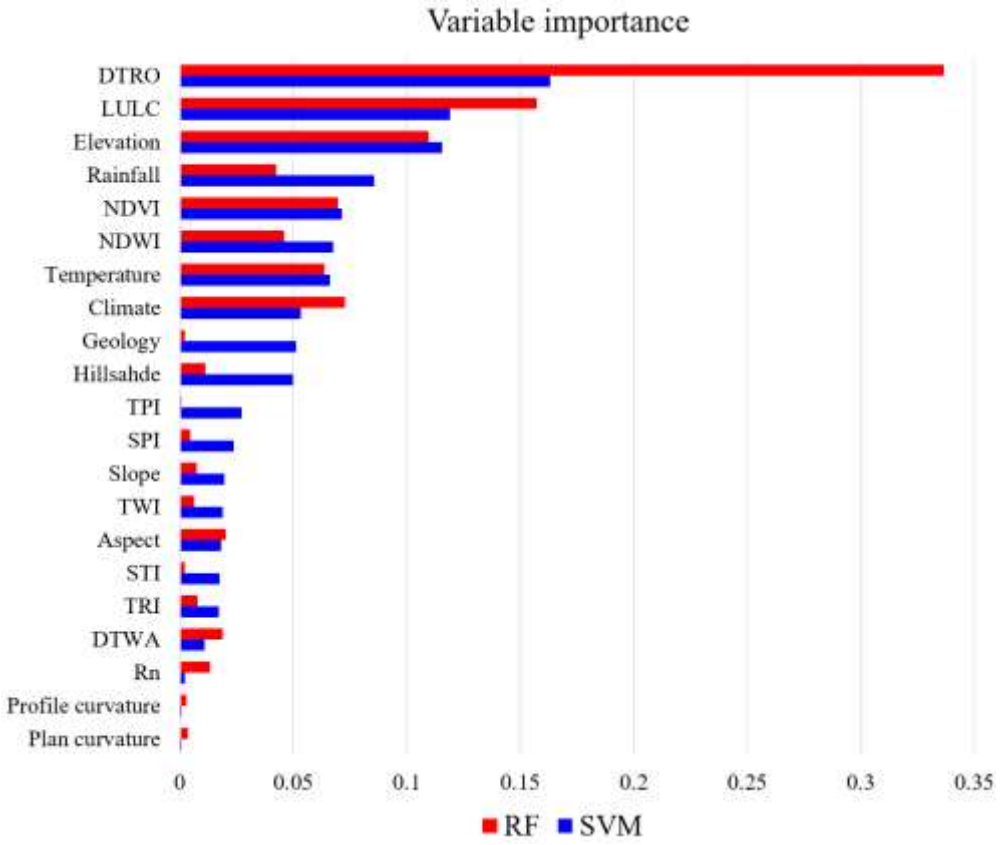

Fig. 10 Variable importance of each landslide conditioning factor in the RF and SVM models.

these maps. The landslide density was calculated for each of the five hazard levels of LSMs. Commonly, the value of landslide density increased progressively, from very low to very high susceptibility (Table 3). Specifically, in the very high susceptibility class, the RF and SVM models generated landslide density values of 6.277 and 4.240, respectively, and the total landslide density values were 6.772 and 5.842, respectively.

By analyzing the RF and SVM algorithms, the variable importance ranges were obtained among the contribution of twenty-one factors to the occurrence of landslides, and the landslide conditioning variables demonstrated varied contributions to the models. Figure 10 presents the variable importance, showcasing the significance of each conditioning factor normalized within the models. Notably, DTRO, LULC, elevation, rainfall, NDVI, NDWI, temperature, and climate emerge as pivotal variables, overshadowing the significance of the remaining conditioning factors in both RF and SVM models.

4.3. PERFORMANCE EVALUATION AND VALIDATION OF LANDSLIDE SUSCEPTIBILITY PREDICTION MODELS

In this research, the training set (80 %) used for the landslide susceptibility prediction model and the testing set (20 %) used for model validation were randomly selected from the observed dataset. The confusion matrixes shown in Figure 11 and Figure12 provide valuable insights into the performance of the RF and SVM models in predicting landslide susceptibility. By analyzing these matrixes, it can be assessed how well each model performs on both the training and testing set, which is crucial for evaluating the generalization capability of the models. On the training set, the RF model exhibits a high true positive (TP) rate with 1899 correctly predicted landslide occurrences and a very low false negative (FN) rate of 167, indicating that the model is efficient in identifying landslides. However, the model also shows a moderate number of false positives (FP) at 299, which means that some areas were incorrectly predicted as landslide-prone. The true negative (TN) rate is 2031, reflecting the model's effectiveness in correctly identifying non-landslide areas (Fig. 11a). On the testing set, the RF model shows the TP rate is 26 and the FN rate is 3. The FP rate is 5, and the TN rate is 28, suggesting that the model still maintains a decent generalization ability (Fig. 11b). On the training set, the SVM model displays 134 TPs and 32 FNs. A TP rate of 134 indicates good sensitivity in detecting landslide occurrences, while a low FN rate of 32 suggests few missed landslides. This indicates that the SVM model performs well on the training data in terms of identifying landslide occurrences. The FP rate is 23, which suggests a low rate of false alarms, while the TN count is 125, which indicates correctly

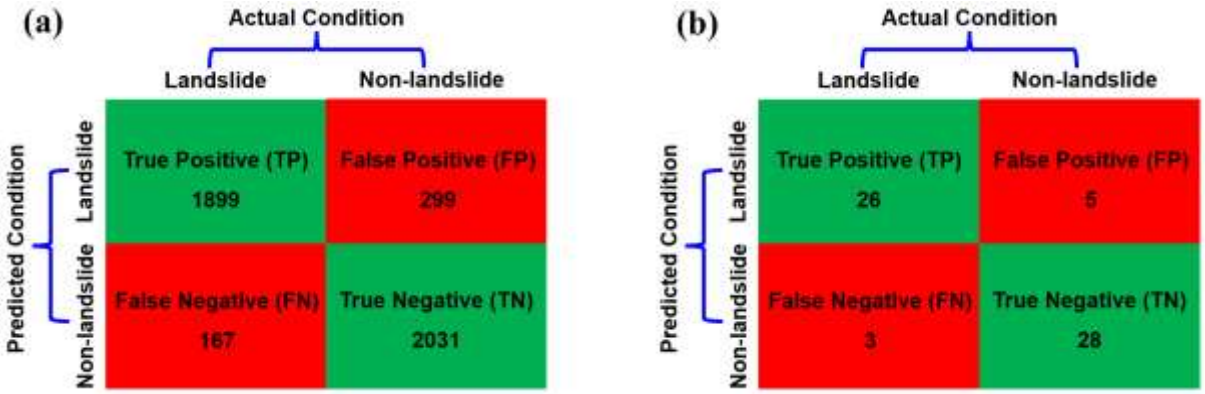

Fig. 11 Confusion matrix of RF model prediction values: (a) training set and (b) testing set.

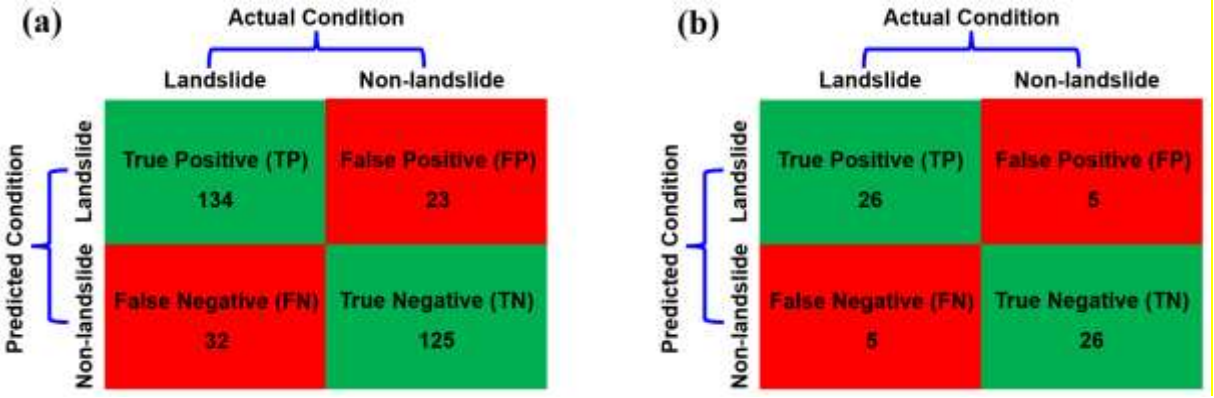

Fig. 12 Confusion matrix of SVM model prediction values: (a) training set and (b) testing set.

Table 4 The evaluation of performance metrics by training set.

	Valuation score			
Model	**Precision**	**Recall**	**F1-Score**	**Accuracy**
RF	0.864	0.919	0.891	0.894
SVM	0.854	0.807	0.830	0.825

identifying non-landslide areas (Fig. 12a). However, SVM indicates it is less effective than the RF model in identifying landslides during training. On the testing set, the SVM model has the same TP count of 26 as the RF model but also has a higher FN count of 5. The FP and TN rates of the SVM model indicate 5 and 26, respectively (Fig. 12b). This suggests that while the SVM model's generalization performance is on par with the RF model, it might be slightly less reliable in accurately predicting landslides. Overall, the RF model appears to perform better than the SVM model, especially in the training phase, as evidenced by its higher TP rate and lower FN rate. However, the SVM model shows fewer FPs, which might be preferable in certain applications where false alarms could be costly. The confusion matrixes for both models on the training and testing sets suggest that both are capable of effective classification, although the RF model exhibits a slight edge in terms of overall accuracy.

The performance evaluation of two predictive models was conducted by various performance metrics such as precision, recall, F1-Score, and accuracy on the training set (Table 4). Precision measures the proportion of correctly predicted landslide occurrences out of all predicted landslide occurrences. A higher precision indicates a lower rate of false positives. The precision value of RF is 0.864, suggesting that 86.4 % of predicted landslide occurrences were indeed landslides. The precision value of SVM is 0.854, indicating a slightly lower precision compared to RF. Recall measures the proportion of correctly predicted landslide events out of all actual landslide occurrences. A higher recall indicates a lower rate of false negatives. The recall value of RF is 0.919, suggesting that 91.9 % of actual landslide occurrences were correctly predicted. The recall value of SVM is 0.807, indicating a lower recall compared to RF, suggesting more missed landslide

Table 5 The evaluation of performance metrics by testing set.

Model	Valuation score			
	Precision	Recall	F1-Score	Accuracy
RF	0.839	0.897	0.867	0.871
SVM	0.839	0.839	0.839	0.839

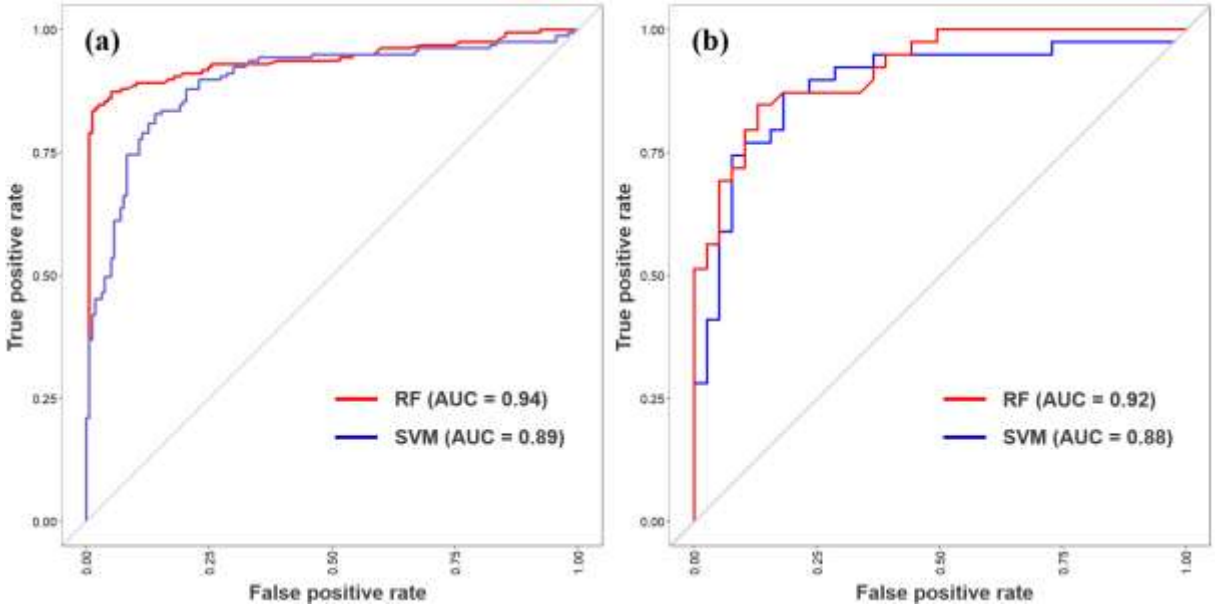

Fig. 13 The ROC curve of RF and SVM models: (a) training set and (b) testing set.

occurrences. F1-Score is the harmonic mean of precision and recall, providing a balanced measure of performance. The F1-Score of RF is 0.891, indicating a good balance between precision and recall. The F1-Score of SVM is 0.830, indicating a lower F1-Score compared to RF, suggesting a trade-off between precision and recall. Accuracy measures the overall proportion of correct predictions. The RF model indicated a high overall accuracy of 0.894. The SVM model indicated a lower overall accuracy of 0.825 compared to RF. Based on the performance evaluation metrics, both RF and SVM models demonstrate reasonable performance in the landslide susceptibility prediction model. However, the RF model generally outperforms the SVM model in terms of precision, recall, F1-Score, and overall accuracy. This suggests that the RF model is better able to identify landslide occurrences and minimize false positives and false negatives.

Then, the performance evaluation on a testing set is evaluated to validate these findings and ensure the landslide susceptibility model's generalizability (Table 5). The precision values reflect the model's capacity to accurately detect positive instances, with the RF model exhibiting a precision of 0.839 and the SVM model at 0.839 also. The recall values indicate the model's ability to correctly identify all positive instances, with RF counting 0.897 and SVM counting 0.839. The RF model achieves a superior F1-Score of 0.867, while the SVM model follows with a score of 0.839. The accuracy metric represents the overall accuracy of the model's predictions, where the RF model outperforms with an accuracy of 0.871 compared to the SVM model at 0.839. Generally, both RF and SVM models exhibit strong performance across all metrics evaluated, with RF slightly greater than SVM in terms of accuracy, precision, recall, and F1-Score. Thus, the RF model demonstrated higher performance in predicting landslide susceptibility compared to the SVM model, as evidenced by higher values in valuation score and accuracy across both the training set and testing set. This presents that RF is more effective in accurately identifying and predicting landslide occurrences in the present research.

Furthermore, the model performance of landslide susceptibility prediction can be evaluated using ROC-AUC values, and a higher AUC value indicates better performance of the model in predicting landslide susceptibility (Ji et al., 2023; Khabiri et al., 2023; Mwakapesa et al., 2023; Sirbu, 2023). The ROC curves and AUC values of the landslide susceptibility prediction by the training set and the ROC curves and AUC values of prediction model validation by the testing set from RF and SVM models are shown in Figure 13a and Figure 13b. In these Figures, the ROC curves were drawn through the x-axis (false positive rate) and y-axis (true positive rate). The ROC and AUC values results (Fig. 13a) showed the

performance of the landslide susceptibility prediction by the RF model is that AUC = 0.94 and the performance of the landslide susceptibility prediction by the SVM model is that AUC = 0.89, respectively. The ROC and AUC values results (Fig. 13b) presented the validation of the RF model is that AUC = 0.92 and the validation of SVM is that AUC = 0.88, respectively. The ROC curves and AUC values are adopted to validate and compare the performance of the two models. It can be certain that the validation rate is perfectly validated for the prediction capability evaluation of the two models' outcomes. Therefore, these two models' entire ROC curves and AUC values had very high predictive performance results, and the models used in this research demonstrated reasonably good accuracy in the spatial prediction of landslide susceptibility. In the comparison of the two models, the analysis of the ROC curves and AUC values results of the RF model have higher AUC (0.94, 0.89) values than the SVM model has 0.92, 0.88 values. So, the RF model exhibited better results for landslide distribution prediction in this research area according to the ROC and AUC values.

4.4. POTENTIAL IMPACT OF SEASONAL VARIATIONS AND CLIMATE CHANGE

Shwe et al. (2023) identified significant correlations between environmental factors, particularly rainfall intensity and landslide occurrences in Chin State, Western Myanmar (Shwe et al., 2024). These findings emphasize the critical influence of seasonal precipitation and climate-induced changes on landslide risks. As climate change continues to alter weather patterns, shifts in rainfall intensity and distribution are expected to exacerbate the frequency and severity of landslides in vulnerable regions like Chin State. This underscores the necessity of integrating climate projections into landslide susceptibility models to better anticipate and mitigate the impacts of future climate scenarios.

In examining the potential impact of seasonal variations and climate change on landslide susceptibility, the LSMs generated for each month of 2024 using both RF and SVM models serve as crucial implements for understanding the temporal distribution of landslide susceptibility. Beyond seasonal rainfall, climate change introduces longer-term shifts in environmental conditions, such as changes in precipitation intensity and the frequency of extreme weather events (Gunasinghe et al., 2023; Mishra et al., 2023; Shou, 2023; Wu, 2024). Consequently, LSMs based on monthly rainfall and climate data offer a more nuanced comprehension of how these temporal fluctuations affect landslide risk.

The total landslide density is derived from these LSMs (Fig. 14) reflecting these variations, as shown in Figure 15. During the cold season, landslide densities were relatively high in both models. The RF model predicted a density of 6.637 in January, whereas the SVM model predicted a slightly lower density of 5.164. The higher density rates during these months suggest that the cold season in Chin State, Myanmar, might still experience moderate landslide activity, potentially due to factors such as winter precipitation, freeze-thaw cycles, and weakened soil stability.

In contrast, during the hot season (February, March, and April), there was a general decrease in landslide density, particularly in the SVM model. The RF model showed a slight decrease in densities, ranging from 6.173 in February to 5.888 in March and 5.822 in April. Meanwhile, the SVM model predicted densities decreasing from 5.285 in February to 4.457 in March and 4.032 in April. This reduction in landslide density may be attributed to the generally dry conditions and reduced precipitation, which can temporarily stabilize the soil and slopes.

The wet season (May, June, and July), characterized by the highest levels of rainfall, exhibited the most significant increase in landslide density. The RF model predicted densities of 6.278 in May, 7.042 in June, and 6.772 in July, while the SVM model forecasted densities of 5.105 in May, 5.697 in June, and 5.842 in July. The substantial rise in landslide density during these months underscores the critical role of heavy monsoon rains in triggering landslides. The saturation of the soil and increased pore-water pressure during the wet season likely contribute to slope failures, making this period the most hazardous in terms of landslide occurrences (Kuriakose et al., 2009; Liu et al., 2022; Zhao et al., 2021).

Although both models indicate similar trends, the specific values and rankings of months differ, suggesting potential variations in their sensitivity to underlying factors. The observed seasonal variations in landslide densities align with the known climatic patterns in Chin State, where the monsoon season is the primary driver of landslides. The higher densities observed during the cold and wet seasons highlight the influence of residual moisture and intense rainfall in this region. With climate change expected to intensify weather patterns, these seasonal trends could become more pronounced. Increased rainfall intensity during the wet season could result in even higher landslide occurrences, while changes in the cold season's freeze-thaw cycles could impact slope stability differently (Gunasinghe et al., 2023; Miklin et al., 2022; Mishra et al., 2023; Shou, 2023; Wu, 2024).

In conclusion, landslide susceptibility in Chin State is strongly influenced by seasonal variations, with the wet season presenting the highest risk. Both RF and SVM models effectively capture these patterns, although the RF model consistently predicts higher landslide densities across all seasons, suggesting its potential superiority in modeling such environmental hazards. This analysis highlights the importance of developing targeted mitigation strategies that account for seasonal and climatic factors to reduce landslide risks in the region.

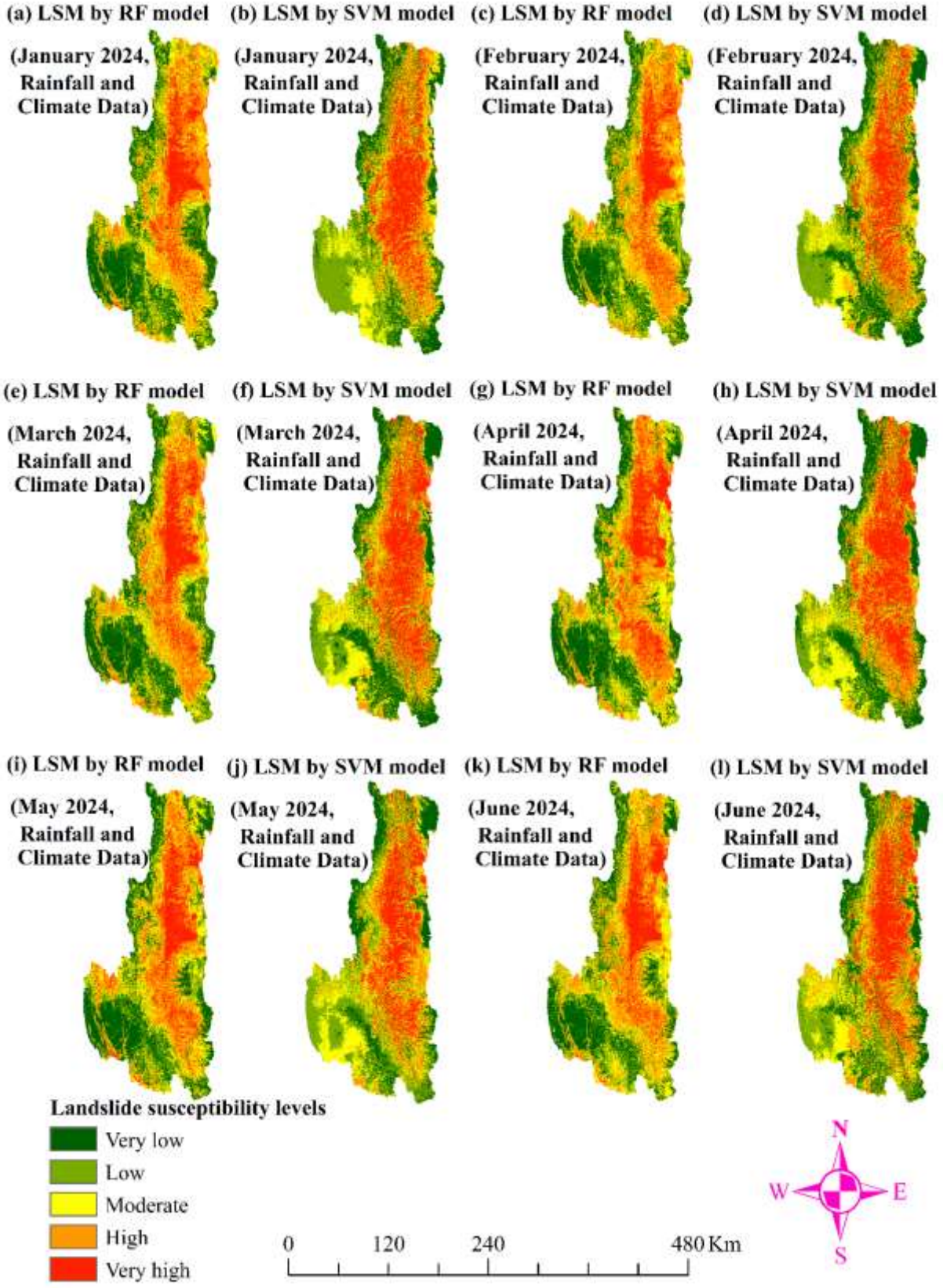

Fig. 14 Landslide susceptibility maps: (a) RF model and (b) SVM model for January 2024, (c) RF model and (d) SVM model for February 2024, (e) RF model and (f) SVM model for March 2024, (g) RF model and (h) SVM model for April 2024, (i) RF model and (j) SVM model for May 2024, and (k) RF model and (l) SVM model for June 2024

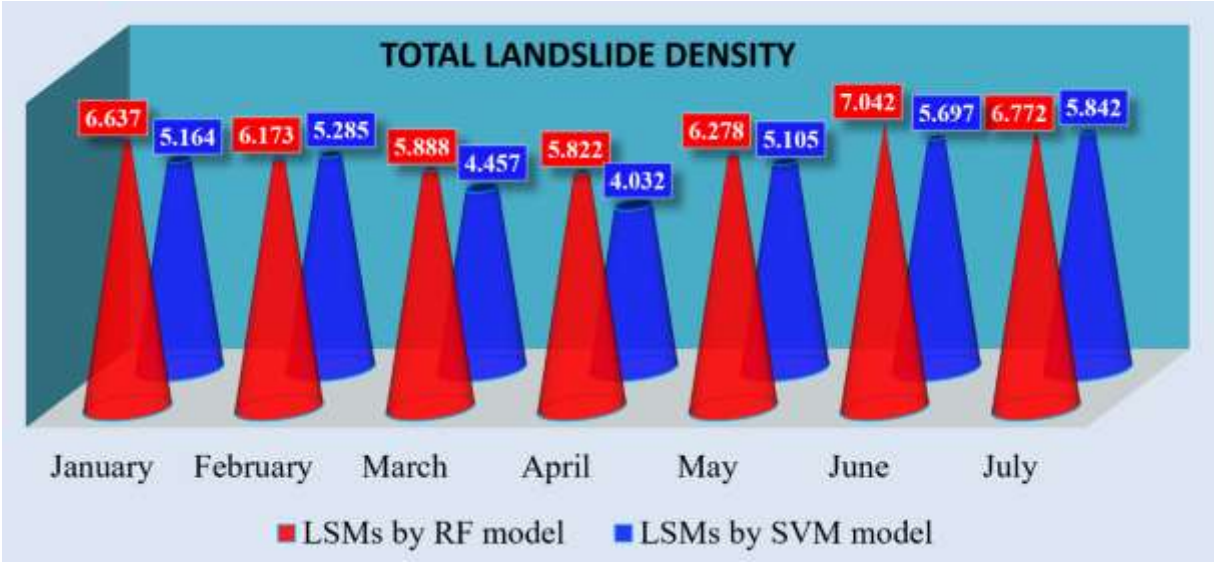

Fig. 15 Total landslide density of LSMs by RF and SVM models.

4.5. REGIONAL LANDSLIDE SUSCEPTIBILITY COMPARISON

Rakhine State, located along the western coast of Myanmar, is geographically positioned between latitudes 17° 20′ 00″ N – 21° 30′ 00″ N and longitudes 92° 00′ 00″ E – 95° 00′ 00″ E, with Chin State to its north and the Bay of Bengal to its west and south, creating a complex environmental setting prone to frequent landslide events, particularly during the rainy season. The prevalent types of landslides that have occurred in this state include circular failure, plane failure, wedge failure, and toppling (UNDP, 2011). The geological structure of Rakhine State is dominated by the Arakan Yoma Mountain range, which is part of the larger Indo-Burman Ranges, similar to Chin State (Kyi Khin et al., 2017). As this state features the Rakhine Yoma, the predominant rock types found in these ranges include thick layers of flysch rocks, metamorphic rocks, metasedimentary rocks, and ultrabasic rocks. The rock layers are tightly folded and inclined towards the east. Significant overthrusts with sloping fault planes are visible in a north-south orientation. The primary factors contributing to landslides in this state include unusually high pore-water pressure, which increases during rainstorms, cutting down of natural vegetation, undercutting erosion, and excavation at the base of slopes (UNDP, 2011). Furthermore, human activities such as deforestation and agricultural practices have intensified soil erosion. The combination of these geological, climatic, and anthropogenic factors creates a complex and challenging environment prone to frequent landslides.

To assess and compare the landslide susceptibility in Rakhine State, the same machine learning models, RF and SVM, were employed as in the study of Chin State. These models were calibrated by using the same set of landslide conditioning factors as those employed in the Chin State analysis. So, the landslide conditioning factors were collected and applied to the specific characteristics of Rakhine State as well. The LSMs were generated for Rakhine State using the RF and SVM models (Fig. 16), and their performance was evaluated using performance metrics such as precision, recall, F1-Score, and accuracy, alongside ROC-AUC values (Table 6). The results demonstrated that both RF and SVM models produced accurate and reliable predictions for landslide susceptibility in Rakhine State, with RF slightly outperforming SVM in most performance metrics.

Table 6 The evaluation of performance metrics and ROC-AUC values by training set and testing set.

Model	Set	Valuation score			Accuracy	ROC-AUC values
		Precision	Recall	F1-Score		
	Training	0.896	0.923	0.909	0.912	0.98
RF	***Testing***	0.860	0.896	0.878	0.882	0.96
	Training	0.786	0.783	0.784	0.787	0.88
SVM	***Testing***	0.840	0.750	0.792	0.784	0.83

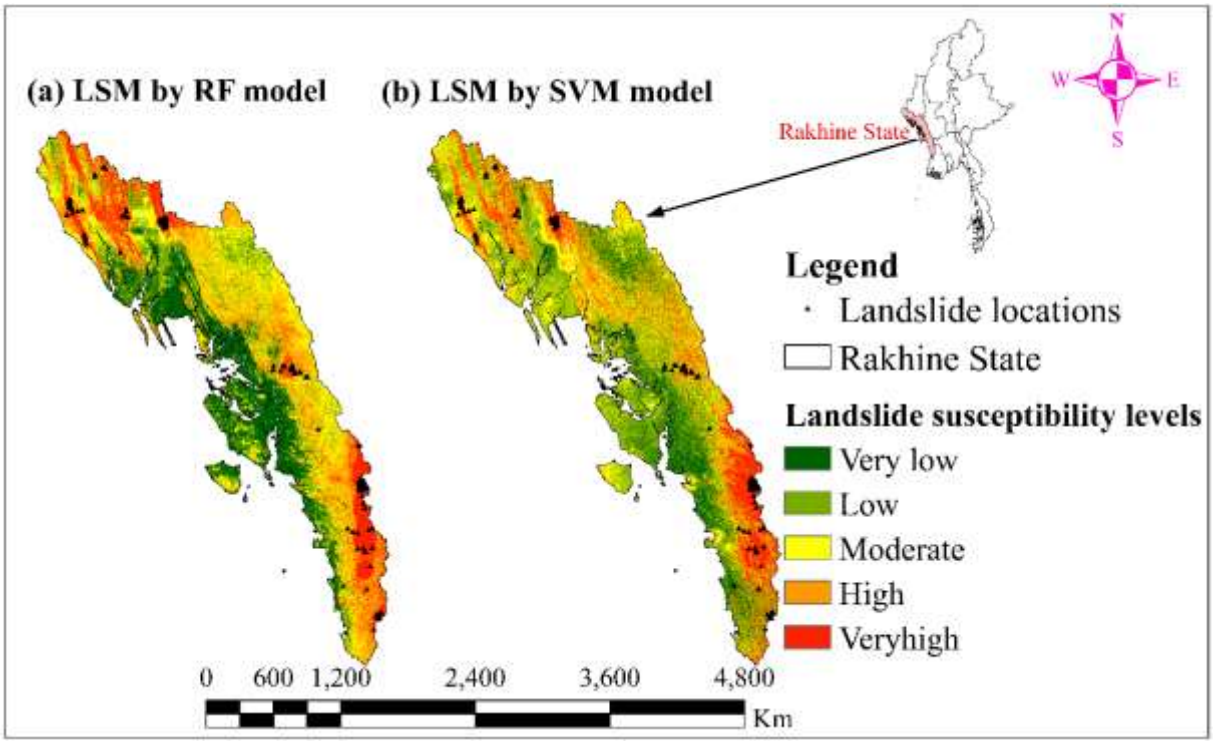

Fig. 16 Landslide susceptibility maps of Rakhine State: (a) RF model and (b) SVM model.

The LSMs for Rakhine State yielded total landslide density values of 7.508 for the RF model and 6.612 for the SVM model, both slightly higher than those observed in Chin State. This difference in landslide density between the two states can be attributed to the distinct geological and environmental characteristics of Rakhine State. The region is dominated by the Rakhine Yoma, which consists of sedimentary rock formations, such as sandstone and shale, that are more prone to weathering and erosion (Kyi Khin et al., 2017). Additionally, the coastal influence of the Bay of Bengal contributes to unique climatic patterns, including high rainfall and frequent cyclonic activities, which exacerbate the risk of landslides. This comparative analysis underscores the models' robustness across different regions and emphasizes the importance of utilizing region-specific geological and environmental contexts in landslide susceptibility modeling.

5. CONCLUSIONS

In this research, two machine learning models such as RF and SVM models were used to identify the GIS-based LSMs for Chin State, Myanmar. An extensive dataset comprising 213 landslide locations and an equal number of randomly chosen non-landslide locations is created for a landslide inventory map. The dataset is randomly divided into a training set (80%) for the landslide susceptibility prediction model and a testing set (20%) for the validation of the model. To analyze landslide susceptibility, twenty-one landslide conditioning factors (i.e., elevation (m), aspect, slope (°), hillshade, plan curvature, profile curvature, TWI, TPI, TRI, Rn, SPI, STI, DTRO (m), DTWA (m), geology, LULC, NDVI, NDWI, temperature (°), rainfall (mm), and climate) were selected. The relationship between each class of landslide conditioning factors and landslide occurrence was conducted by FR analysis. The LSMs generated by FR and SVM landslide susceptibility prediction models were divided into five susceptibility classes: very low, low, moderate, high, and very high.

The RF and SVM landslide susceptibility prediction models were evaluated using performance metrics, including precision, recall, F1-Score, and accuracy, based on the training set. The RF model achieved a precision of 0.864, indicating that 86.4 % of the predicted landslide instances were accurate. In contrast, the SVM model had a slightly lower precision of 0.854. The recall of the RF model was 0.919, meaning that it successfully identified 91.9 % of the actual landslide occurrences, whereas the SVM model had a recall of 0.807, suggesting a higher rate of missed landslides. The F1-Score, which balances precision and recall, was 0.891 for the RF model, reflecting a strong performance, while the SVM model had an F1-Score of 0.830, indicating a less optimal balance. The overall accuracy of the RF model was high at 0.894, surpassing the SVM model's accuracy of 0.825. These metrics demonstrate that while both models are effective for landslide susceptibility prediction modeling, the RF model consistently performs better across all metrics, making it the more reliable option for predicting landslides in this research.

The validation of the two predictive models by the testing set is subsequently assessed through performance metrics such as precision, recall, F1-

Score, and accuracy on the testing set. The precision values serve to indicate the capability of models in correctly identifying positive instances: RF = 0.839 and SVM = 0.839. In parallel, the recall values represent the accurate identification of all positive instances: RF = 0.897 and SVM = 0.839. Furthermore, the F1-Score, functioning as the harmonic mean of precision and recall, serves to balance the overall performance of the models: RF = 0.867 and SVM = 0.839. The metric of accuracy demonstrates the accuracy of model predictions: RF = 0.871 and SVM = 0.839. Ultimately, the RF model showcases the most robust performance across all metrics, with the RF model slightly surpassing the SVM model concerning precision, recall, F1-Score, and accuracy.

The ROC and AUC values quantitatively indicate the performance, accuracy, and validation of landslide susceptibility prediction models. The AUC results indicated that the RF model achieved an AUC of 0.94 for the training set and 0.92 for the testing set, while the SVM model attained AUC values of 0.89 for the training set and 0.88 for the testing set. It can be concluded that these two-hybrid landslide susceptibility prediction model analyses had satisfactory results and exhibited reasonably good accuracy for LSMs in this research area. Consequently, any of these models can be useful for spatial prediction of landslide susceptibility within this research area. Specifically, the RF model yielded better outcomes than the SVM model in the comparison of the ROC curve and AUC values. Therefore, it can be said that the LSM generated by the RF model has best performed in this research area according to performance metrics (i.e., accuracy, precision, recall, and F1-Score) and the ROC and AUC values.

The completion of LSMs showed susceptibility was predominantly concentrated in the northern and northeastern zones of the state for landslide occurrence. The outcomes of this research hold significance for initial land use planning and future hazard mitigation, offering valuable insights for decision-makers and ultimately aiding in the creation of effective strategies for managing hazards. Furthermore, the concepts and methods of this research can serve as a reference for assessing landslide susceptibility in other specific areas in the future, aiding in the management of landslide risks and supporting sustainable development initiatives.

AUTHOR CONTRIBUTIONS

All authors contributed to the study's conception and design. Material preparation, data collection, and analysis were performed by Soe Hlaing Tun. The first draft of the manuscript was written by Soe Hlaing Tun. Manuscript editing and proofreading were completed by Farhad Jamil. Zeng Changnv commented on previous versions of the manuscript, and all manuscript was reviewed and supervised by Zeng Changnv. All authors read and approved the final manuscript.

FUNDING

The authors did not receive support from any organization for the submitted work.

REFERENCES

Abdo, H.G., Almohamad, H., Al Dughairi, A.A.and Ali, S.A., Parvin, F., Elbeltagi, A., Costache, R., Mohammed, S., Al-Mutiry, M. and Alsafadi, K.: 2022, Spatial implementation of frequency ratio, statistical index and index of entropy models for landslide susceptibility mapping in Al-Balouta river basin, Tartous Governorate, Syria. Geosci. Lett. 9, 45. DOI:10.1186/s40562-022-00256-5

Achu, A.L., Thomas, J., Aju, C.D., Remani, P.K. and Gopinath, G.: 2023, Performance evaluation of machine learning and statistical techniques for modelling landslide susceptibility with limited field data. Earth Sci. Inform. 16, 1025–1039. DOI: 10.1007/s12145-022-00910-8

Achu, A.L., Thomas, J., Aju, C.D., Vijith, H. and Gopinath, G.: 2024, Redefining landslide susceptibility under extreme rainfall events using deep learning. Geomorphology, 448, 109033. DOI: 10.1016/j.geomorph.2023.109033

Addis, A.: 2023, GIS-based landslide susceptibility mapping using frequency ratio and shannon entropy models in Dejen District, Northwestern Ethiopia. J. Eng. 2023, 1–14. DOI: 10.1155/2023/1062388

Aggarwal, C.C.: 2023, Neural networks and deep learning: A textbook. Springer International Publishing, Cham. DOI: 10.1007/978-3-031-29642-0

Akinci, H. and Yavuz Ozalp, A.: 2021, Landslide susceptibility mapping and hazard assessment in Artvin (Turkey) using frequency ratio and modified information value model. Acta Geophys., 69, 725–745. DOI: 10.1007/s11600-021-00577-7

Ali, S.A., Parvin, F., Vojteková, J., Costache, R., Linh, N.T.T., Pham, Q.B., Vojtek, M., Gigović, L., Ahmad, A. and Ghorbani, M.A.: 2021, GIS-based landslide susceptibility modeling: A comparison between fuzzy multi-criteria and machine learning algorithms. Geosci. Front., 12, 857–876. DOI: 10.1016/j.gsf.2020.09.004

Althuwaynee, O.F., Pradhan, B., Park, H.-J. and Lee, J.H.: 2014, A novel ensemble bivariate statistical evidential belief function with knowledge-based analytical hierarchy process and multivariate statistical logistic regression for landslide susceptibility mapping. CATENA, 114, 21–36. DOI: 10.1016/j.catena.2013.10.011

Altunel, A.O.: 2023, The effect of DEM resolution on topographic wetness index calculation and visualization: An insight to the hidden danger unraveled in Bozkurt in August, 2021. Int. J. Eng. Geosci., 8, 165–172. DOI: 10.26833/ijeg.1110560

Alvioli, M., Mondini, A.C., Fiorucci, F., Cardinali, M. and Marchesini, I.: 2018, Topography-driven satellite imagery analysis for landslide mapping. Geomat. Nat. Hazards Risk, 9, 544–567. DOI: 10.1080/19475705.2018.1458050

Amah, E.M., Katte, V.Y., Ghogomu, R.T. and Kamgang, V.K.: 2022, An assessment of landslides along mountain forest roads: Bamenda ring road segment through Bafut and Befang Forests on the Cameroon Volcanic Line. Am. J. Environ. Stud., 5, 60–86. DOI: 10.47672/ajes.1160

Anis, Z., Wissem, G., Vali, V., Smida, H. and Mohamed Essghaier, G.: 2019, GIS-based landslide

susceptibility mapping using bivariate statistical methods in North-western Tunisia. Open Geosci., 11, 708–726. DOI: 10.1515/geo-2019-0056

Arabameri, A., Pradhan, B., Rezaei, K. and Lee, C.-W.: 2019, Assessment of landslide susceptibility using statistical- and artificial intelligence-based FR–RF integrated model and multiresolution DEMs. Remote Sens., 11, 999. DOI: 10.3390/rs11090999

Arabameri, A., Saha, S., Roy, J., Chen, W., Blaschke, T. and Tien Bui, D.: 2020, Landslide susceptibility evaluation and Management Using Different Machine Learning Methods in The Gallicash River Watershed, Iran. Remote Sens. 12, 475. DOI: 10.3390/rs12030475

Arca, D., Keskin Citiroglu, H. and Tasoglu, I.K.: 2019, A comparison of GIS-based landslide susceptibility assessment of the Satuk village (Yenice, NW Turkey) by frequency ratio and multi-criteria decision methods. Environ. Earth Sci., 78, 81. DOI: 10.1007/s12665-019-8094-6

Ashournejad, Q., Hosseini, A., Pradhan, B. and Hosseini, S.J.: 2019, Hazard zoning for spatial planning using GIS-based landslide susceptibility assessment: a new hybrid integrated data-driven and knowledge-based model. Arab. J. Geosci., 12, 126. DOI: 10.1007/s12517-019-4236-0

Azarafza, M., Hajialilue Bonab, M. and Derakhshani, R.: 2022, A deep learning method for the prediction of the index mechanical properties and strength parameters of Marlstone. Materials, 15, 6899. DOI: 10.3390/ma15196899

Badola, S., Mishra, V.N. and Parkash, S.: 2023, Landslide susceptibility mapping using XGBoost machine learning method. In: 2023 International Conference on Machine Intelligence for GeoAnalytics and Remote Sensing (MIGARS). IEEE, Hyderabad, India, 1–4. DOI: 10.1109/MIGARS57353.2023.10064496

Bai, S.-B., Wang, J., Lü, G.-N., Zhou, P.-G., Hou, S.-S. and Xu, S.-N.: 2009, GIS-based and data-driven bivariate landslide-swusceptibility mapping in the Three Gorges Area, China. Pedosphere, 19, 14–20. DOI: 10.1016/S1002-0160(08)60079-X

Biau, G.: 2012, Analysis of a random forests model. J. Mach. Learn. Res., 13, 1063-1095.

Bostjančić, I., Filipović, M., Gulam, V. and Pollak, D.: 2021, Regional-scale landslide susceptibility mapping using limited LiDAR-based landslide inventories for Sisak-Moslavina County, Croatia. Sustainability, 13, 4543. DOI: 10.3390/su13084543

Botchkarev, A.: 2019, A new typology design of performance metrics to measure errors in machine learning regression algorithms. Interdiscip. J. Inf. Knowl. Manag., 14, 045–076. DOI: 10.28945/4184

Breiman, L.: 2001, Random forests. Mach. Learn., 45, 5–32. DOI: 10.1023/A:1010933404324

Burkov, A.: 2019, The hundred-page machine learning book, 141 pp.

Sivakami, C. and Rajkumar, R.: 2020, Landslide vulnerability zone by weights of evidence model using remote sensing and GIS, in Kodaikanal Taluk (Tamil nadu, India). Int. J. Eng. Res., V9, IJERTV9IS020201. DOI: 10.17577/IJERTV9IS020201

Chapi, K., Singh, V.P., Shirzadi, A., Shahabi, H., Bui, D.T., Pham, B.T. and Khosravi, K.: 2017, A novel hybrid artificial intelligence approach for flood susceptibility assessment. Environ. Model. Softw., 95, 229–245. DOI: 10.1016/j.envsoft.2017.06.012

Chen, C., Liaw, A. and Breiman, L.: 2004, Using random forest to learn imbalanced data University of California, Berkeley.

Chen, W. and Li, Y.: 2020, GIS-based evaluation of landslide susceptibility using hybrid computational intelligence models. CATENA, 195, 104777. DOI: 10.1016/j.catena.2020.104777

Chen, W., Sun, Z. and Han, J.: 2019, Landslide susceptibility modeling using integrated ensemble weights of evidence with logistic regression and random forest models. Appl. Sci., 9, 171. DOI: 10.3390/app9010171

Chen, W., Zhang, S., Li, R. and Shahabi, H.: 2018, Performance evaluation of the GIS-based data mining techniques of best-first decision tree, random forest, and naïve Bayes tree for landslide susceptibility modeling. Sci. Total Environ., 644, 1006–1018. DOI: 10.1016/j.scitotenv.2018.06.389

Chen, X. and Chen, W.: 2021, GIS-based landslide susceptibility assessment using optimized hybrid machine learning methods. CATENA, 196, 104833. DOI: 10.1016/j.catena.2020.104833

Chowdhury, Md.S.: 2023, Modelling hydrological factors from DEM using GIS. MethodsX, 10, 102062. DOI: 10.1016/j.mex.2023.102062

Chowdhury, R., Flentje, P. and Bhattacharya, G.: 2013, Geotechnics in the twenty-first century, uncertainties and other challenges: With particular reference to landslide hazard and risk assessment. In: Chakraborty, S. and Bhattacharya, G. (Eds.), Proc. the International Symposium on Engineering under Uncertainty: Safety Assessment and Management (ISEUSAM - 2012). Springer India, India, 27–53. DOI: 10.1007/978-81-322-0757-3_2

Christmann, A. and Steinwart, I.: 2008, Support vector machines. Springer New York. DOI: 10.1007/978-0-387-77242-4

Chueasamat, A., Hori, T., Saito, H., Sato, T. and Kohgo, Y.: 2018, Experimental tests of slope failure due to rainfalls using 1g physical slope models. Soils Found., 58, 290–305. DOI: 10.1016/j.sandf.2018.02.003

Cristianini, N. and Shawe-Taylor, J.: 2000, An introduction to support vector machines and other kernel-based learning methods, 1st ed. Cambridge University Press. DOI: 10.1017/CBO9780511801389

Cutler, D.R., Edwards, T.C., Beard, K.H., Cutler, A., Hess, K.T., Gibson, J. and Lawler, J.J.: 2007, Random forests for classification in ecology. Ecology, 88, 2783–2792. DOI: 10.1890/07-0539.1

Dahal, R.K., Hasegawa, S., Nonomura, A., Yamanaka, M., Masuda, T. and Nishino, K.: 2008, GIS-based weights-of-evidence modelling of rainfall-induced landslides in small catchments for landslide susceptibility mapping. Environ. Geol., 54, 311–324. DOI: 10.1007/s00254-007-0818-3

Das, G. and Lepcha, K.: 2019, Application of logistic regression (LR) and frequency ratio (FR) models for landslide susceptibility mapping in Relli Khola river basin of Darjeeling Himalaya, India. SN Appl. Sci., 1, 1453. DOI: 10.1007/s42452-019-1499-8

Das, J., Saha, P., Mitra, R., Alam, A. and Kamruzzaman, M.: 2023, GIS-based data-driven bivariate statistical models for landslide susceptibility prediction in Upper Tista Basin, India. Heliyon, 9, e16186. DOI: 10.1016/j.heliyon.2023.e16186

Davies, T.: 2015, Landslide hazards, risks, and disasters. Elsevier, 1–16. DOI: 10.1016/B978-0-12-396452-6.00001-X

Demir, G., Aytekin, M., Akgün, A., İkizler, S.B. and Tatar, O.: 2013, A comparison of landslide susceptibility mapping of the eastern part of the North Anatolian Fault Zone (Turkey) by likelihood-frequency ratio and analytic hierarchy process methods. Nat. Hazards, 65, 1481–1506. DOI: 10.1007/s11069-012-0418-8

Devkota, K.C., Regmi, A.D., Pourghasemi, H.R., Yoshida, K., Pradhan, B., Ryu, I.C., Dhital, M.R. and Althuwaynee, O.F.: 2013, Landslide susceptibility mapping using certainty factor, index of entropy and logistic regression models in GIS and their comparison at Mugling–Narayanghat road section in Nepal Himalaya. Nat. Hazards, 65, 135–165. DOI: 10.1007/s11069-012-0347-6

Dixon, N., Smith, A. and Pietz, M.: 2022, A community-operated landslide early warning approach: Myanmar case study. Geoenvironmental Disasters, 9, 18. DOI: 10.1186/s40677-022-00220-7

Dou, J., Yunus, A.P., Tien Bui, D., Sahana, M., Chen, C.-W., Zhu, Z., Wang, W. and Pham, B.T.: 2019, Evaluating GIS-based multiple statistical models and data mining for earthquake and rainfall-induced landslide susceptibility using the LiDAR DEM. Remote Sens., 11, 638. DOI: 10.3390/rs11060638

Du, G., Zhang, Y., Iqbal, J., Yang, Z. and Yao, X.: 2017, Landslide susceptibility mapping using an integrated model of information value method and logistic regression in the Bailongjiang watershed, Gansu Province, China. J. Mt. Sci., 14, 249–268. DOI: 10.1007/s11629-016-4126-9

Ferri, C., Hernández-Orallo, J. and Modroiu, R.: 2009, An experimental comparison of performance measures for classification. Pattern Recognit. Lett., 30, 27–38. DOI: 10.1016/j.patrec.2008.08.010

Gao, B.: 1996, NDWI–A normalized difference water index for remote sensing of vegetation liquid water from space. Remote Sens. Environ., 58, 257–266. DOI: 10.1016/S0034-4257(96)00067-3

Gao, J., Shi, X., Li, L., Zhou, Z. and Wang, J.: 2022, Assessment of landslide susceptibility using different machine learning methods in Longnan City, China. Sustainability, 14, 16716. DOI: 10.3390/su142416716

Ghasemian, B., Shahabi, H., Shirzadi, A., Al-Ansari, N., Jaafari, A., Kress, V.R., Geertsema, M., Renoud, S. and Ahmad, A.: 2022, A robust deep-learning model for landslide susceptibility mapping: A case study of Kurdistan Province, Iran. Sensors, 22, 1573. DOI: 10.3390/s22041573

Gigović, L., Drobnjak, S. and Pamučar, D.: 2019, The application of the hybrid GIS spatial multi-criteria decision analysis best–worst methodology for landslide susceptibility mapping. ISPRS Int. J. Geo-Inf., 8, 79. DOI: 10.3390/ijgi8020079

Gomes, R., Denton, A. and Franzen, D.: 2019, Comparing classification accuracy of NDVI with DEM derived attributes using multi-scalar approach in geographic information systems. In: 2019 IEEE International Conference on Electro Information Technology (EIT). Brookings, SD, USA, 249–254. DOI: 10.1109/EIT.2019.8833766

Gopi, B., Premalatha, J., Kalaivani, R. and Ravikumar, D.: 2023a, Cloud based landslide detection and alerting nearby people by using IoT technology. In: 2023 Third International Conference on Artificial Intelligence and Smart Energy (ICAIS). ~~Presented at the 2023 Third~~ Coimbatore, India, 1287–1292. DOI: 10.1109/ICAIS56108.2023.10073773

Gorsevski, P.V., Brown, M.K., Panter, K., Onasch, C.M., Simic, A. and Snyder, J.: 2016, Landslide detection and susceptibility mapping using LiDAR and an artificial neural network approach: a case study in the Cuyahoga Valley National Park, Ohio. Landslides, 13, 467–484. DOI: 10.1007/s10346-015-0587-0

Gunasinghe, L., Gunawardhana, L. and Rajapakse, L.: 2023, Predictive analysis of landslide susceptibility under hydrological aspects of climate change in Kegalle District, Sri Lanka. In: 2023 Moratuwa Engineering Research Conference (MERCon). ~~P.~~ IEEE, Moratuwa, Sri Lanka,-119–124. DOI: 10.1109/MERCon60487.2023.10355394

Guo, Z., Shi, Y., Huang, F., Fan, X. and Huang, J.: 2021, Landslide susceptibility zonation method based on C5.0 decision tree and K-means cluster algorithms to improve the efficiency of risk management. Geosci. Front., 12, 101249. DOI: 10.1016/j.gsf.2021.101249

Guzzetti, F., Reichenbach, P., Ardizzone, F., Cardinali, M. and Galli, M.: 2006, Estimating the quality of landslide susceptibility models. Geomorphology, 81, 166–184. DOI: 10.1016/j.geomorph.2006.04.007

Habib, M.: 2021, Evaluation of DEM interpolation techniques for characterizing terrain roughness. CATENA, 198, 105072. DOI: 10.1016/j.catena.2020.105072

Hand, D.J.: 2012, Assessing the performance of classification methods. Int. Stat. Rev., 80, 400–414. DOI: 10.1111/j.1751-5823.2012.00183.x

Hart, A.: 2024, Landslides, in Ciottone's Disaster Medicine. Elsevier, 640–643. DOI: 10.1016/B978-0-323-80932-0.00104-X

He, K., Ma, G., Hu, X. and Liu, B.: 2021, Failure mechanism and stability analysis of a reactivated landslide occurrence in Yanyuan City, China. Landslides, 18, 1097–1114. DOI: 10.1007/s10346-020-01571-8

Hong, H., Shahabi, H., Shirzadi, A., Chen, W., Chapi, K., Ahmad, B.B., Roodposhti, M.S., Yari Hesar, A., Tian, Y. and Tien Bui, D.: 2019, Landslide susceptibility assessment at the Wuning area, China: a comparison between multi-criteria decision making, bivariate statistical and machine learning methods. Nat. Hazards, 96, 173–212. DOI: 10.1007/s11069-018-3536-0

Hsu, C.W., Chang, C.C. and Lin, C.J.: 2016, A practical guide to support vector classification.

Hua, Y., Wang, X., Li, Y., Xu, P. and Xia, W.: 2021, Dynamic development of landslide susceptibility based on slope unit and deep neural networks. Landslides, 18, 281–302. DOI: 10.1007/s10346-020-01444-0

Hung, P.V., Son, P.Q. and Dung, N.V.: 2016, The study evaluated arming of risk of lanslide in Hoa Binh and Son La reservoir hydropower area on the basis of analyzing high-resolution remote sensing and geographic information systems. Vietnam J. Earth. Sci., 37, 193–203. DOI: 10.15625/0866-7187/37/3/7792

Ji, J., Zhou, Y., Cheng, Q., Jiang, S. and Liu, S.: 2023, Landslide susceptibility mapping based on deep learning algorithms using information value analysis optimization. Land, 12, 1125. DOI: 10.3390/land12061125

Kannan, M., Saranathan, E. and Anabalagan, R.: 2013, Landslide vulnerability mapping using frequency ratio model: a geospatial approach in Bodi-Bodimettu Ghat section, Theni district, Tamil Nadu, India. Arab. J. Geosci., 6, 2901–2913. DOI: 10.1007/s12517-012-0587-5

Kavzoglu, T. and Colkesen, I.: 2009, A kernel functions analysis for support vector machines for land cover classification. Int. J. Appl. Earth Obs. Geoinf., 11, 352–359. DOI: 10.1016/j.jag.2009.06.002

Khabiri, S., Crawford, M.M., Koch, H.J., Haneberg, W.C. and Zhu, Y.: 2023, An assessment of negative samples

and model structures in landslide susceptibility characterization based on Bayesian network models. Remote Sens., 15, 3200. DOI: 10.3390/rs15123200

Khan, H., Shafique, M., Khan, M.A., Bacha, M.A., Shah, S.U. and Calligaris, C.: 2019, Landslide susceptibility assessment using Frequency Ratio, a case study of northern Pakistan. Egypt. J. Remote Sens. Space Sci., 22, 11–24. DOI: 10.1016/j.ejrs.2018.03.004

Kopecký, M., Macek, M. and Wild, J.: 2021, Topographic wetness index calculation guidelines based on measured soil moisture and plant species composition. Sci. Total Environ., 757, 143785. DOI: 10.1016/j.scitotenv.2020.143785

Kormann, M. and Lock, G.: 2014, Exploring the effects of curvature and refraction on GIS-based visibility studies, In: Verhagen, P. and Earl, G. (Eds.), Archaeology in the digital era. Amsterdam University Press, 428–437. DOI: 10.1515/9789048519590-046

Kunwar, B.B., Muensit, N., Techato, K. and Gyawali, S.: 2023, Landslide susceptibility mapping of phewa watershed, Kaski, Nepal. DOI: 10.21203/rs.3.rs-2860742/v1

Kuriakose, S.L., Sankar, G. and Muraleedharan, C.: 2009, History of landslide susceptibility and a chorology of landslide-prone areas in the Western Ghats of Kerala, India. Environ. Geol., 57, 1553–1568. DOI: 10.1007/s00254-008-1431-9

Kwon, S., Pan, L., Kim, Y., Lee, S.I., Kweon, H., Lee, K., Yeom, K. and Seo, J.I.: 2023, Empirical comparison of supervised learning methods for assessing the stability of slopes adjacent to military operation roads. Forests, 14, 1237. DOI: 10.3390/f14061237

Kyaw Htun, Cho Thae Oo, Tun Naing Zaw and Day Wa Aung.: 2019, Landslide hazard in Chin State: A case study in Hakka and its environs. Population, Development, and the Environment. Springer Nature Singapore, Singapore, 195–213. DOI: 10.1007/978-981-13-2101-6_12

Kyi Khin, Khin Zaw and Lin Thu Aung.: 2017, Geological and tectonic evolution of the Indo-Myanmar Ranges (IMR) in the Myanmar region. Geol. Soc. Lond. Mem., 48, 65–79. DOI: 10.1144/M48.4

Latuamury, B., Talaohu, M., Sahusilawane, F. and Imlabla, W.N.: 2021, Correlation of normalized difference water index and baseflow index in small island watershed landscapes. IOP Conf. Ser. Earth Environ. Sci., 883, 012072. DOI: 10.1088/1755-1315/883/1/012072

LeCun, Y., Bengio, Y. and Hinton, G.: 2015, Deep learning. Nature, 521, 436–444. DOI: 10.1038/nature14539

Lei, X., Chen, W., Pham, B.T.: 2020, Performance evaluation of GIS-based artificial intelligence approaches for landslide susceptibility modeling and spatial patterns analysis. ISPRS Int. J. Geo-Inf., 9, 443. DOI: 10.3390/ijgi9070443

Liaw, A. and Wiener, M., 2002, Classification and regression by random forest. R News, 2, 3, 18–22.

Liu, J., Xu, Q., Wang, S., Siva Subramanian, S., Wang, L. and Qi, X.: 2020, Formation and chemo-mechanical characteristics of weak clay interlayers between alternative mudstone and sandstone sequence of gently inclined landslides in Nanjiang, SW China. Bull. Eng. Geol. Environ., 79, 4701–4715. DOI: 10.1007/s10064-020-01859-y

Liu, Y., Yuan, A., Bai, Z. and Zhu, J.: 2022, GIS-based landslide susceptibility mapping using frequency ratio and index of entropy models for She County of Anhui Province, China. Appl. Rheol., 32, 22–33. DOI: 10.1515/arh-2022-0122

Loche, M. and Scaringi, G.s 2024, Exploring temperature-shear strength dynamics: A spatial modelling approach for clay landslide susceptibility in Italy. DOI: 10.5194/egusphere-egu24-5190

Loche, M., Scaringi, G. and Lombardo, L.: 2022, Land surface temperature controls stability in gentle clay slopes. DOI: 10.5194/icg2022-411

Maodin, M.A., Faryansah, Ariadi, S.D., Verlandi, G.S., Alpiana, Hidayati.: 2023, Analysis of andesite rock slope stability with bishop method. IOP Conf. Ser. Earth Environ. Sci., 1175, 012007. DOI: 10.1088/1755-1315/1175/1/012007

May Thu, N., Mar Mar Aye and Kyaw Lwin, O.: 2022, Rainfall and landslide susceptibility in Hakha environ in Northern Chin State, Myanmar. Br. J. Arts Humanit., 1–14. DOI: 10.34104/bjah.02201014

Meena, S.R., Puliero, S., Bhuyan, K., Floris, M., Catani, F.: 2022, Assessing the importance of conditioning factor selection in landslide susceptibility for the province of Belluno (region of Veneto, northeastern Italy). Nat. Hazards Earth Syst. Sci., 22, 1395–1417. DOI: 10.5194/nhess-22-1395-2022

Miklin, L., Podolszki, L., Gulam, V. and Markotić, I.: 2022, The impact of climate changes on slope stability and landslide conditioning factors: An example from Kravarsko, Croatia. Remote Sens., 14, 1794. DOI: 10.3390/rs14081794

Mishra, A.N., Maraun, D., Knevels, R., Truhetz, H., Brenning, A. and Proske, H.: 2023, Climate change amplified the 2009 extreme landslide event in Austria. Clim. Change, 176, 124. DOI: 10.1007/s10584-023-03593-2

Mukherjee, I. and Singh, U.K.: 2020, Delineation of groundwater potential zones in a drought-prone semi-arid region of east India using GIS and analytical hierarchical process techniques. CATENA, 194, 104681. DOI: 10.1016/j.catena.2020.104681

Muller, A.C. and Guido, S.: 2016, Introduction to machine learning with Python: a guide for data scientists. Sebastopol, CA, O'Reilly Media, Inc.

Mwakapesa, D.S., Lan, X., Nanehkaran, Y.A. and Mao, Y.: 2023, Landslide susceptibility mapping using O-CURE and PAM clustering algorithms. Front. Environ. Sci., 11, 1140834. DOI: 10.3389/fenvs.2023.1140834

Nadim, F., Kjekstad, O., Peduzzi, P., Herold, C. and Jaedicke, C.: 2006, Global landslide and avalanche hotspots. Landslides, 3, 159–173. DOI: 10.1007/s10346-006-0036-1

Neogi, S., Dasgupta, S. and Fukuoka, M.: 1998, High P-T polymetamorphism, dehydration melting, and generation of migmatites and granites in the higher Himalayan crystalline complex, Sikkim, India. J. Petrol., 39, 61–99. DOI: 10.1093/petroj/39.1.61

Nhu, V.-H., Hoang, N.-D., Nguyen, H., Ngo, P.T.T., Thanh Bui, T., Hoa, P.V., Samui, P. and Tien Bui, D.: 2020a, Effectiveness assessment of Keras based deep learning with different robust optimization algorithms for shallow landslide susceptibility mapping at tropical area. CATENA, 188, 104458. DOI: 10.1016/j.catena.2020.104458

Nhu, V.-H., Shirzadi, A., Shahabi, H., Chen, W., Clague, J.J., Geertsema, M., Jaafari, A., Avand, M., Miraki, S., Talebpour Asl, D., Pham, B.T., Ahmad, B.B. and Lee, S.: 2020b, Shallow landslide susceptibility mapping by random forest base classifier and its ensembles in a Semi-Arid Region of Iran. Forests, 11, 421. DOI: 10.3390/f11040421

Nsengiyumva, J.B., Luo, G., Amanambu, A.C., Mind'je, R., Habiyaremye, G., Karamage, F., Ochege, F.U. and Mupenzi, C.: 2019, Comparing probabilistic and statistical methods in landslide susceptibility modeling in Rwanda/Centre-Eastern Africa. Sci. Total Environ., 659, 1457–1472. DOI: 10.1016/j.scitotenv.2018.12.248

Pal, S.C. and Chowdhuri, I.: 2019, GIS-based spatial prediction of landslide susceptibility using frequency ratio model of Lachung River basin, North Sikkim, India. SN Appl. Sci., 1, 416. DOI: 10.1007/s42452-019-0422-7

Paryani, S., Neshat, A., Javadi, S. and Pradhan, B.: 2020, Comparative performance of new hybrid ANFIS models in landslide susceptibility mapping. Nat. Hazards, 103, 1961–1988. DOI: 10.1007/s11069-020-04067-9

Pham, B.T., Jaafari, A., Prakash, I. and Bui, D.T.: 2019, A novel hybrid intelligent model of support vector machines and the MultiBoost ensemble for landslide susceptibility modeling. Bull. Eng. Geol. Environ., 78, 2865–2886. DOI: 10.1007/s10064-018-1281-y

Pham, B.T., Khosravi, K. and Prakash, I.: 2017, Application and comparison of decision tree-based machine learning methods in landside susceptibility assessment at Pauri Garhwal Area, Uttarakhand, India. Environ. Process., 4, 711–730. DOI: 10.1007/s40710-017-0248-5

Pham, B.T., Tien Bui, D. and Prakash, I.: 2018a, Bagging based support vector machines for spatial prediction of landslides. Environ. Earth Sci., 77, 146. DOI: 10.1007/s12665-018-7268-y

Pham, B.T., Tien Bui, D. and Prakash, I.: 2018b, Bagging based Support Vector Machines for spatial prediction of landslides. Environ. Earth Sci. 77, 146. DOI: 10.1007/s12665-018-7268-y

Platt, J.C.: 2000, Probabilistic outputs for support vector machines and comparisons to regularized likelihood methods.

Poudyal, C.P., Chang, C., Oh, H.-J. and Lee, S.: 2010, Landslide susceptibility maps comparing frequency ratio and artificial neural networks: a case study from the Nepal Himalaya. Environ. Earth Sci., 61, 1049–1064. DOI: 10.1007/s12665-009-0426-5

Pourghasemi, H.R. and Kerle, N.: 2016, Random forests and evidential belief function-based landslide susceptibility assessment in Western Mazandaran Province, Iran. Environ. Earth Sci., 75, 185. DOI: 10.1007/s12665-015-4950-1

Prasad, P., Loveson, V.J., Das, S. and Chandra, P.: 2021, Artificial intelligence approaches for spatial prediction of landslides in mountainous regions of western India. Environ. Earth Sci., 80, 720. DOI: 10.1007/s12665-021-10033-w

R M, Y., Dolui, B.: 2021, Statistical and machine intelligence based model for landslide susceptibility mapping of Nilgiri district in India. Environ. Chall., 5, 100211. DOI: 10.1016/j.envc.2021.100211

Rana, S.: 2006, Use of plan curvature variations for the identification of ridges and channels on DEM. Progress in Spatial Data Handling. Springer Berlin Heidelberg, 789–804. DOI: 10.1007/3-540-35589-8_49

Rani, R., Benini, A., Foschi, A. and Berti, M.: 2023, Stability of a rock slope overlying a weak clay: the difficult case of Balze di Verghereto (Italy). DOI: 10.5194/egusphere-egu23-7815

Regmi, N.R., Giardino, J.R. and Vitek, J.D.: 2010, Modeling susceptibility to landslides using the weight of evidence approach: Western Colorado, USA. Geomorphology, 115, 172–187. DOI: 10.1016/j.geomorph.2009.10.002

Reichenbach, P., Rossi, M., Malamud, B.D., Mihir, M. and Guzzetti, F.: 2018, A review of statistically-based landslide susceptibility models. Earth-Sci. Rev., 180, 60–91. DOI: 10.1016/j.earscirev.2018.03.001

Rodriguez, J., Macciotta, R., Hendry, M.T., Roustaei, M., Gräpel, C. and Skirrow, R.: 2020, UAVs for monitoring, investigation, and mitigation design of a rock slope with multiple failure mechanisms—a case study. Landslides, 17, 2027–2040. DOI: 10.1007/s10346-020-01416-4

Roy, D., Sarkar, A., Kundu, P., Paul, S. and Chandra Sarkar, B.: 2023, An ensemble of evidence belief function (EBF) with frequency ratio (FR) using geospatial data for landslide prediction in Darjeeling Himalayan region of India. Quat. Sci. Adv., 11, 100092. DOI: 10.1016/j.qsa.2023.100092

Saad, M., Kamel, M. and Moftah, H.: 2024, Landslide susceptibility mapping for the Red Sea Mountains: A multi-criteria decision analysis approach. J. Afr. Earth Sci., 209, 105125. DOI: 10.1016/j.jafrearsci.2023.105125

Samui, P.: 2008, Slope stability analysis: a support vector machine approach. Environ. Geol., 56, 255–267. DOI: 10.1007/s00254-007-1161-4

Sarker, I.H.: 2021, Deep learning: A comprehensive overview on techniques, taxonomy, applications and research directions. SN Comput. Sci., 2, 420. DOI: 10.1007/s42979-021-00815-1

Scaringi, G., Loche, M., Tourchi, S. and Lombardo, L.: 2022, Temperature and slope stability in temperate climate. DOI: 10.5194/egusphere-plinius17-26

Schuster, R.L. and Wieczorek, G.F.: 2018, Landslide triggers and types, Landslides. Routledge, 59–78. DOI: 10.1201/9780203749197-4

Shahabi, H., Ahmadi, R., Alizadeh, M., Hashim, M., Al-Ansari, N., Shirzadi, A., Wolf, I.D. and Ariffin, E.H.: 2023, Landslide susceptibility mapping in a mountainous area using machine learning algorithms. Remote Sens., 15, 3112. DOI: 10.3390/rs15123112

Shou, K.-J.: 2023, Landslide susceptibility and resilience changing climate– for the case in Taiwan. DOI: 10.5194/egusphere-egu23-1949

Shwe, M.M., Yeboah, E., Okrah, A., Sarfo, I., Oo, K.L., Moe, A.H.H., Takin, M., Prempeh, N.A., Mensah, C., Kwang, C., Bhatta, D. and Djan, M.A.: 2024, Multi-factor analysis of landslide and flood occurrences in Chin State, Western Myanmar. Eur. J. Environ. Earth Sci., 5, 1–11. DOI: 10.24018/ejgeo.2024.5.3.459

Singha, C. and Swain, K.C.: 2022, Evaluating the NDVI based rice and potato yield prediction map using GIS geostatistical environment. In: 2022 Second International Conference on Advances in Electrical, Computing, Communication and Sustainable Technologies (ICAECT). Bhilai, India, 1–7. DOI: 10.1109/ICAECT54875.2022.9807981

Sirbu, F.: 2023, Landslide susceptibility model based on random forest classification. DOI: 10.5194/egusphere-egu23-733

Sun, D., Xu, J., Wen, H. and Wang, Y.: 2020, An optimized random forest model and its generalization ability in landslide susceptibility mapping: Application in two areas of Three Gorges Reservoir, China. J. Earth Sci., 31, 1068–1086. DOI: 10.1007/s12583-020-1072-9

Taalab, K., Cheng, T. and Zhang, Y.: 2018, Mapping landslide susceptibility and types using random forest. Big Earth Data, 2, 159–178. DOI: 10.1080/20964471.2018.1472392

Thakur, N. and Sharma, Dr.S.: 2022, Study of sustainable techniques for effective risk management and control: A review. Int. J. Res. Appl. Sci. Eng. Technol., 10, 1688–1696. DOI: 10.22214/ijraset.2022.44121

Thi Ngo, P.T., Panahi, M., Khosravi, K., Ghorbanzadeh, O., Kariminejad, N., Cerda, A. and Lee, S.: 2021, Evaluation of deep learning algorithms for national scale landslide susceptibility mapping of Iran. Geosci. Front., 12, 505–519. DOI: 10.1016/j.gsf.2020.06.013

Tien Bui, D., Tuan, T.A., Klempe, H., Pradhan, B. and Revhaug, I.: 2016, Spatial prediction models for shallow landslide hazards: a comparative assessment of the efficacy of support vector machines, artificial neural networks, kernel logistic regression, and logistic model tree. Landslides, 13, 361–378. DOI: 10.1007/s10346-015-0557-6

Tin Tin, N., Robinson, S.A., Searle, M.P., Morley, C.K., Millar, I., Green, O.R., Bown, P.R., Danelian, T., Petrizzo, M.R. and Henderson, G.M.: 2023, Age, depositional history and tectonics of the Indo-Myanmar Ranges, Myanmar. J. Geol. Soc., 180, jgs2022-091. DOI: 10.1144/jgs2022-091

Tsangaratos, P. and Ilia, I.: 2016, Landslide susceptibility mapping using a modified decision tree classifier in the Xanthi Perfection, Greece. Landslides, 13, 305–320. DOI: 10.1007/s10346-015-0565-6

UNDP.: 2011, Multi hazard risk assessment in the Rakhine State of Myanmar.

United Nations Team.: 1979, Geological Survey and Exploration Technical Report 4. United Nations Development Programme, New York.

Wang, H., Zhang, L., Yin, K., Luo, H. and Li, J.: 2021, Landslide identification using machine learning. Geosci. Front., 12, 351–364. DOI: 10.1016/j.gsf.2020.02.012

Wang, L.-J., Guo, M., Sawada, K., Lin, J. and Zhang, J.: 2016, A comparative study of landslide susceptibility maps using logistic regression, frequency ratio, decision tree, weights of evidence and artificial neural network. Geosci. J., 20, 117–136. DOI: 10.1007/s12303-015-0026-1

Wang, Q., Guo, Y., Li, W., He, J. and Wu, Z.: 2019, Predictive modeling of landslide hazards in Wen County, northwestern China based on information value, weights-of-evidence, and certainty factor. Geomat. Nat. Hazards Risk, 10, 820–835. DOI: 10.1080/19475705.2018.1549111

Wang, Q., Li, W., Chen, W. and Bai, H.: 2015, GIS-based assessment of landslide susceptibility using certainty factor and index of entropy models for the Qianyang County of Baoji city, China. J. Earth Syst. Sci., 124, 1399–1415. DOI: 10.1007/s12040-015-0624-3

Winzeler, H.E., Owens, P.R., Read, Q.D., Libohova, Z., Ashworth, A. and Sauer, T.: 2022, Topographic wetness index as a proxy for soil moisture in a hillslope catena: Flow algorithms and map generalization. Land, 11, 2018. DOI: 10.3390/land11112018

Woodard, J.B., Mirus, B.B., Crawford, M.M., Or, D., Leshchinsky, B.A., Allstadt, K.E. and Wood, N.J.: 2023, Mapping landslide susceptibility over large regions with limited data. J. Geophys. Res. Earth Surf., 128, e2022JF006810.DOI: 10.1029/2022JF006810

Wu, C.: 2024, Assessment of landslide susceptibility under climate change in the Laonong river watershed in Taiwan. DOI: 10.5194/egusphere-egu24-3729

Wu, Y., Li, W., Liu, P., Bai, H., Wang, Q., He, J., Liu, Y. and Sun, S.: 2016, Application of analytic hierarchy process model for landslide susceptibility mapping in the Gangu County, Gansu Province, China. Environ. Earth Sci., 75, 422. DOI: 10.1007/s12665-015-5194-9

Wubalem, A.: 2022, Landslide inventory, susceptibility, hazard and risk mapping, landslides. IntechOpen. DOI: 10.5772/intechopen.100504

Wubalem, A. and Meten, M.: 2020, Landslide susceptibility mapping using information value and logistic regression models in Goncha Siso Eneses area, northwestern Ethiopia. SN Appl. Sci., 2, 807. DOI: 10.1007/s42452-020-2563-0

Xiong, X., Shi, Z., Xiong, Y., Peng, M., Ma, X. and Zhang, F.: 2019, Unsaturated slope stability around the Three Gorges Reservoir under various combinations of rainfall and water level fluctuation. Eng. Geol., 261, 105231. DOI: 10.1016/j.enggeo.2019.105231

Yang, G., Liang, S., Gui, X., Xie, Y. and Zhao, H.: 2019, Optimizing landslide susceptibility mapping in the Kongtong District, NW China: comparing the subdivision criteria of factors. Geocarto Int., 34, 1408–1426. DOI: 10.1080/10106049.2018.1499816

Yasukuni, O. and Soe, M.: 2017, Report of life with landslides in Myanmar.

Zha, Y., Gao, J. and Ni, S.: 2003, Use of normalized difference built-up index in automatically mapping urban areas from TM imagery. Int. J. Remote Sens., 24, 583–594. DOI: 10.1080/01431160304987

Zhan, J., Wang, Q., Zhang, W., Shangguan, Y., Song, S. and Chen, J.: 2019, Soil-engineering properties and failure mechanisms of shallow landslides in soft-rock materials. CATENA, 181, 104093. DOI: 10.1016/j.catena.2019.104093

Zhang, S., Li, Z., Hou, X. and Yi, Y.: 2019, Impacts on watershed-scale runoff and sediment yield resulting from synergetic changes in climate and vegetation. CATENA, 179, 129–138. DOI: 10.1016/j.catena.2019.04.007

Zhang, W., Li, H., Han, L., Chen, L. and Wang, L.: 2022, Slope stability prediction using ensemble learning techniques: A case study in Yunyang County, Chongqing, China. J. Rock Mech. Geotech. Eng., 14, 1089–1099. DOI: 10.1016/j.jrmge.2021.12.011

Zhang, Y. and Ling, C.: 2018, A strategy to apply machine learning to small datasets in materials science. Npj Comput. Mater., 4, 25. DOI: 10.1038/s41524-018-0081-z

Zhao, Z., Liu, Z.Y. and Xu, C.: 2021, Slope unit-based landslide susceptibility mapping using certainty factor, support vector machine, random forest, CF-SVM and CF-RF models. Front. Earth Sci., 9, 589630. DOI: 10.3389/feart.2021.589630

Zhou, C., Wang, Yue, Cao, Y., Singhc, R.P., Ahmed, B., Motagh, M., Wang, Yang, Chen, L.: 2023, Non-landslide sampling and ensemble learning techniques to improve landslide susceptibility mapping. DOI: 10.5194/nhess-2023-44

Zhou, C., Yin, K., Cao, Y., Ahmed, B., Li, Y. and Catani, F., Pourghasemi, H.R.: 2018, Landslide susceptibility modeling applying machine learning methods: A case study from Longju in the Three Gorges Reservoir area, China. Comput. Geosci., 112, 23–37. DOI: 10.1016/j.cageo.2017.11.019